A role for Hmga2 in the early-stage transition of neural stem-progenitor cell properties during mouse neocortical development

Naohiro Kuwayama[1,6], Yusuke Kishi[1,6,*], Yurie Maeda[1], Yurie Nishiumi[1], Yutaka Suzuki[2], Haruhiko Koseki[3], Yusuke Hirabayashi[4], and Yukiko Gotoh[1,5,*]

[1]Graduate School of Pharmaceutical Sciences, The University of Tokyo, Tokyo 113-0033, Japan

[2]Department of Computational Biology, Graduate School of Frontier Sciences, The University of Tokyo, Chiba 277-8561, Japan

[3]Laboratory for Developmental Genetics, RIKEN Center for Integrative Medical Sciences (RIKEN-IMS), Tsurumi-ku, Yokohama 230-0045, Japan

[4]Graduate School of Engineering, The University of Tokyo, Tokyo 113-0033, Japan

[5]International Research Center for Neurointelligence (WPI-IRCN), The University of Tokyo, Tokyo 113-0033, Japan

[6]These authors contributed equally

*Correspondence: ykisi@mol.f.u-tokyo.ac.jp, ygotoh@mol.f.u-tokyo.ac.jp

Abstract

During the early stage of mammalian neural development, neuroepithelial cells (NECs) proliferate and increase their pool size before switching their fate to become neurogenic radial glial cells (RGCs). The timing of this expansion-to-neurogenic phase transition is strictly regulated so as to determine the proper number of progenitors and differentiated cell types that constitute the brain. The molecular mechanism underlying this switch has remained poorly understood, however. We have now performed a transcriptomic analysis of NECs and RGCs and found that the expression of *Hmga2* gene, which encodes a chromatin-associated protein, peaks at the expansion-to-neurogenic phase transition. By the use of our newly established method to manipulate NECs before neural tube closure, we found that knockdown of Hmga2 in NECs delayed the change in their transcriptomic profile and suppressed the onset of neurogenesis in the neocortex. Our study thus uncovers a key molecular player in the generation of neurogenic progenitors in the developing mouse neocortex.

Introduction

The neocortex is the seat of higher cognitive function and has undergone evolutionary expansion in mammals. It originates from a pseudostratified sheet of neuroepithelium present at the anterior end of the neural plate before formation of the neural tube. In the course of neocortical development, neural progenitors undergo sequential waves of expansion, neurogenic and gliogenic phases (Gotz and Huttner, 2005; Hirabayashi and Gotoh, 2010; Kriegstein and Alvarez-Buylla, 2009; Mukhtar and Taylor, 2018). During the expansion phase, neural progenitors, also known as neuroepithelial cells (NECs), divide symmetrically to give rise to two progenitors per division (Rakic, 1995). This symmetric division increases the progenitor pool and results in lateral expansion of the neocortex. At the onset of neurogenesis in the mouse neocortex, NECs transform into neurogenic radial glial cells (RGCs), which mainly divide asymmetrically to give rise to one progenitor and one neuron or neuron-committed intermediate progenitor cell per division (Gao et al., 2014; Gotz and Huttner, 2005; Hartfuss et al., 2001; Miyata et al., 2002; Noctor et al., 2001). The elongated basal (radial) processes of RGCs also support the migration of newborn neurons to the pial surface, which results in radial expansion of the neocortex (Rakic, 1972). Clonal analysis of the mouse neocortex has revealed that a neurogenic RGC typically produces 8~9 cortical excitatory neurons through asymmetric division and then transforms into a gliogenic RGC (Gao et al., 2014). To avoid confusion, we will hereafter use the term neural stem-progenitor cells (NPCs) for both NECs and RGCs, given that many, if not all, of these cells are neural stem cells that self-renew and eventually produce both neurons and glial cells and that various nomenclatures are currently in use in the field.

The expansion-to-neurogenic phase (E-to-N) transition of NPC fate takes place at around embryonic day (E) 10 in the mouse neocortex. The timing of this E-to-N transition is key to determination of the number of neurons generated and the size of the cortex, given that the duration of the expansion phase determines the size of the founder NPC pool for corticogenesis. With regard to the mechanism of this transition, certain secreted (extrinsic) factors have been found to play a role, with one such factor being all-*trans* retinoic acid (atRA) released from the meninges. In mice, a reticulum of meningeal cells covers the neocortex between E9 and E10 (McLone and Bondareff, 1975) and secretes atRA, which promotes the onset of neurogenesis while suppressing

71 neuroepithelial elongation (Siegenthaler et al., 2009). Fibroblast growth factor (FGF) 10
72 is transiently expressed in anterior NPCs from E9.5 to E11.5 and, together with its
73 receptor FGFR2, also promotes the E-to-N transition in the anterior portion of the
74 neocortex (Sahara and O'Leary, 2009; Yoon et al., 2004). Moreover, an increase in
75 oxygen concentration as a result of periventricular ingrowth of blood vessels from E10.5
76 to E12.5 also appears to be associated with the E-to-N transition (Lange et al., 2016). A
77 recent report also suggests a role of $GABA_AR$ ligands, GABA and taurine, in the E-to-N
78 transition (Tochitani et al., 2021). In addition to these extrinsic factors, cell-intrinsic
79 programs likely regulate the E-to-N transition, given that in vitro cultures of mouse
80 cortical NPCs as well as of human embryonic stem (ES) cell– or primate induced
81 pluripotent stem (iPS) cell–derived NPCs undergo a directional transition from
82 proliferative (symmetric) to differentiating (asymmetric) divisions (Eiraku et al., 2008;
83 Gaspard et al., 2008; Otani et al., 2016; Qian et al., 1998; Shen et al., 2006; Shi et al.,
84 2012). The molecular basis of cell-intrinsic programs that regulate the E-to-N transition
85 of NPC fate (in particular, the timing of this transition) has remained largely unclear,
86 however. Only a few candidate intracellular mechanisms, such as those involving Notch-
87 Hes signaling, the BAF chromatin-remodeling complex and ZEB2, a regulator for
88 epithelial-mesenchymal transition (Anthony et al., 2005; Benito-Kwiecinski et al., 2021;
89 Gaiano et al., 2000; Hatakeyama et al., 2004; Nguyen et al., 2018), have been proposed
90 to date.

91 One possible reason that the molecular basis of the E-to-N transition has
92 remained relatively unexplored compared with that of neurogenesis or gliogenesis later
93 in development is the difficulty of gene manipulation at this early stage of brain
94 development. At late embryonic stages (from ~E12), a gene of interest can be readily
95 introduced into neocortical NPCs by in utero electroporation of plasmids (Tabata and
96 Nakajima, 2001) or by injection of recombinant viruses into the ventricles. However,
97 these methods cannot be applied to earlier stages before the E-to-N transition (such as at
98 E8.0) because neural tube closure does not take place until E8.5 to E9.5 in the mouse
99 forebrain (so there is no ventricle at E8.0) and the presumptive neocortex is too small to
100 manipulate. In this study, we therefore established a simple method for the introduction
101 of a gene of interest into ectodermal (and endodermal) cells of mouse embryos as early
102 as E7.0 or E8.0. This method is based on in utero injection of viral vectors directly into
103 amniotic fluid, given that the neural tube is still open at this early stage. This method,

which is simpler than a similar and recently-published method (Mangold et al., 2021), thus enabled us to examine possible roles of candidate genes related to the E-to-N transition.

A hallmark of NPCs in the neurogenic phase is their neurogenic potential—that is, they maintain an undifferentiated state but are able to differentiate into neurons in response to appropriate cues. The chromatin state of NPCs underlies this neurogenic potential (Kishi and Gotoh, 2018; Nakagawa et al., 2020; Tsuboi et al., 2019). For instance, Polycomb group (PcG) proteins underlie temporary and more persistent repression of neurogenic genes in NPCs during the neurogenic phase and the gliogenic phase, respectively, through distinct molecular mechanisms (Hirabayashi et al., 2009; Tsuboi et al., 2018). High mobility group A (Hmga) proteins 1 and 2 are also chromatin modifiers that contribute to neurogenic potential by regulating the expression of neurogenesis-related genes in NPCs during the neurogenic phase (Fujii et al., 2013; Kishi et al., 2012; Sakai et al., 2019). The levels of Hmga proteins in NPCs are high in the neurogenic phase but gradually decrease during later neocortical development (Kishi et al., 2012; Nishino et al., 2008; Sanosaka et al., 2008), with this decline accounting in part for the loss of neurogenic potential in gliogenic NPCs (Kishi et al., 2012). However, it has remained unknown whether Hmga proteins play a role in the E-to-N transition of NPC fate in the early embryonic mouse neocortex.

In this study, we have identified Hmga2 as a key regulator of the E-to-N transition in the early stage of neocortical development. We found that *Hmga2* expression in neocortical NPCs peaks at around the E-to-N transition (at E10), and that knockdown of Hmga2 from E8.0 with the use of our newly established method delayed the onset of neurogenesis and shifted the transcriptional profile of NPCs at this transition closer to that in the expansion phase. Our results suggest that an increase in Hmga2 expression helps the transition of NPC properties at the onset of the neurogenic phase.

Results

Development of a simple and efficient method for manipulation of gene expression in mouse embryos before neural tube closure

To investigate the E-to-N transition in the mouse neocortex, we set out to develop a simple and efficient method for the introduction of a gene of interest before neural tube closure, ideally before E8.5. To this end, instead of the ultrasound microscopy system adopted in previously reported methods (Gaiano et al., 1999; Mangold et al., 2021), we used an optical fiber to visualize the inner structure of the uterus including the amnion and embryo (Figure 1a-d). Optical fiber–based visualization of the ventricles of embryos from E9.5 was previously described for targeted DNA injection and electroporation after neural tube closure (Matsui et al., 2011). We found that lighting with this system was sufficient to allow injection of a dye inside the amnion, although it was not possible to directly see the amnion within the uterus. We first injected carboxyfluorescein succinimidyl ester (CFSE), a cell-permeable dye that becomes fluorescent after reaction with intracellular proteins (Quah and Parish, 2010; Telley et al., 2016), into the uterus at E8.0 (Figure 1e and f) To minimize possible damage caused by the injection, we inserted a sharpened capillary at the center of the uterus at an angle perpendicular to the uterine wall while it was positioned as shown in Figure 1d. We injected a small volume (~0.5 μl) of solution at a depth of 1 to 2 mm below the uterine wall, which reproducibly resulted in transfer of the solution into the amniotic fluid. The time of surgery is relatively short (~20 min) because of the simplicity of the method, which may contribute to the minimal damage caused to embryos. After 3 days (at E11.0), fluorescence microscopy without sectioning revealed that 77% of injected embryos were labeled with CFSE (Figure 1e and f). About 80% of embryos survived without gross developmental malformations at E11.0. We also injected CFSE into amniotic fluid at E7.0, which again yielded a high rate of embryo labeling (64%) and a high rate of survival without gross developmental malformation (89%) at E9.0 (Figure 1f).

We next performed gene introduction via retroviral vectors with this method. We first injected a concentrated suspension of a retrovirus encoding green fluorescent protein (GFP) into the uterus at E8.0, and we found that 89% of embryos survived without gross abnormalities and that 74% of embryos expressed GFP at E11.0 (Figure 2a and c). Injection of the retrovirus at E7.0 also yielded GFP-expressing embryos at E9.0 (Figure

164 2b and c). Flow cytometric analysis of cortical tissue obtained from E12.0 embryos that
165 had been injected with the retrovirus for GFP at E8.0 showed that ~70% of the cortical
166 cells were positive for GFP in successful cases (Figure 2d). Immunohistofluorescence
167 analysis of sagittal sections of E10.0 embryos that had been injected with the retrovirus
168 encoding GFP at E8.0 revealed that most tissues exposed to amniotic fluid expressed GFP
169 (Figure 2e–g). The labeled tissues thus included the central nervous system (forebrain,
170 midbrain, hindbrain, and spinal cord) as well as the epidermis and endodermal tissues
171 such as those of digestive and respiratory organs. These results suggested that our method
172 is also suitable for gene introduction into such ectodermal and endodermal tissues at this
173 early stage of mouse development.
174 Given that in utero electroporation of plasmids is in general superior to
175 retroviral infection as a means of gene introduction with regard to efficiency and
176 expression level, we next injected a plasmid encoding mCherry with our new method and
177 performed in utero electroporation with the use of electrodes (disc size, 2.5 by 4 mm)
178 positioned on each side of the uterus at E7.0 or E8.0. The fraction of mCherry-expressing
179 embryos at E9.0 and E10.0 was 19% and 40% among those electroporated at E7.0 and
180 E8.0, respectively (Figure 2h and i). The expression pattern of mCherry differed among
181 embryos, likely because of differences in the orientation of the electrodes relative to the
182 embryo during electroporation. Most embryos expressed mCherry in somites (Figure 2h),
183 whereas another manifested mCherry expression in the midbrain and hindbrain (data not
184 shown). No embryo examined to date was found to express mCherry in the forebrain.
185 These results showed that it was possible to perform gene introduction by in utero
186 electroporation in mouse embryos at E7.0 or E8.0 with our method for plasmid injection,
187 although further improvements will be necessary to allow targeting of a specific tissue
188 with this method.
189
190 **Transcriptional profiling of NPCs in the mouse telencephalon during early**
191 **development**
192 To investigate the molecular basis of the E-to-N transition, we first examined changes in
193 the transcriptional profile of NPCs around this developmental stage by RNA-sequencing
194 (RNA-seq) analysis. Given that the E-to-N transition takes place at ~E10 in mice, we
195 isolated NPCs as cells expressing the NPC marker CD133 (also known as prominin-1) at
196 a high level (CD133^{high} cells) from the entire telencephalon at E8.0 and E9.0 and from the

197 neocortex at E10.0, E11.0, and E12.0 by fluorescence-activated cell sorting (FACS)
198 (Figure 3a). Hierarchical clustering analysis of differentially expressed genes (defined by
199 *maSigPro* of the *R* package) revealed five clusters based on the pattern of the expression
200 changes (Figure 3b–f, Supplemental Data 1). The genes in cluster 1 showed a decline in
201 expression level, most prominently from E8.0 to E10.0 (Figure 3b), whereas those in
202 cluster 3 showed an increase in expression level, most prominently from E10.0 to E12.0
203 (Figure 3d). Gene ontology (GO) analysis showed that the genes in cluster 1 were
204 enriched in those related to tissue morphogenesis and embryo development (Figure 3b),
205 whereas the genes in cluster 3 were enriched in those related to nervous system
206 development and generation of neurons (Figure 3d). These findings confirmed the proper
207 isolation of NPCs at each stage. The genes in clusters 2 and 4 were potentially associated
208 with the E-to-N transition (~E10), given that their expression levels decreased and
209 increased, respectively, predominantly from E9.0 to E11.0 (Figure 3c and e). The genes
210 in cluster 2 were enriched in those related to ribosome biogenesis and RNA processing
211 (Figure 3c), suggesting that these processes might be regulated differentially in the
212 expansion versus neurogenic phase. Ribosome biogenesis has indeed been found to be
213 attenuated in NPCs at around this stage (Chau et al., 2018), again providing support for
214 the proper isolation of NPCs for this analysis. The enrichment of genes related to RNA
215 processing in cluster 2 is of interest, given the pivotal role of such processing in the
216 control of NPC differentiation (Yoon et al., 2017; Zahr et al., 2018; Zhang et al., 2016).
217 The genes in cluster 4 were enriched in those related to cell projection and cell
218 morphogenesis (Figure 3e), possibly reflecting the dynamic morphological changes of
219 NPCs as they transition from NECs to RGCs.
220 The genes in cluster 5 may be particularly relevant to the E-to-N transition,
221 given that their expression peaks at E10.0 (Figure 3f). We therefore hypothesized that this
222 cluster includes genes that promote the E-to-N transition. The top five highly expressed
223 genes of cluster 5 at E10.0 are shown in Figure 3g. Among them, we focused on *Hmga2*,
224 given that Hmga proteins have been shown to confer neurogenic potential on mouse
225 neocortical NPCs at late developmental stages (Kishi et al., 2012). However, the possible
226 role of Hmga2 at early developmental stages—in particular, at the E-to-N transition—has
227 remained unknown.
228
229 **Hmga2 promotes the onset of neurogenesis in the mouse neocortex**

230 We first confirmed the temporal expression pattern of *Hmga2* in NPCs by RT-qPCR
231 analysis, which again showed a peak at E10.0 (Figure 2h), whereas those of the early-
232 stage NEC marker *Lin28b* and the RGP marker *Glast* showed an increase and a decrease
233 from E8.0 to E12.0, respectively (Supplementary Figure 1a). To investigate the relevance
234 of the increase in the level of *Hmga2* expression in neocortical NPCs at this particular
235 embryonic stage, we knocked down Hmga2 with the use of a specific short hairpin RNA
236 (shRNA) from E8.0 with our method for early embryo manipulation. We introduced
237 retroviruses encoding GFP and shRNAs specific either for Hmga2 or for luciferase
238 (control) into NPCs at E8.0 and analyzed the embryos at E10.0 and E11.0 (Figure 4a).
239 RT-qPCR and immunohistofluorescence analyses confirmed the depletion of *Hmga2*
240 mRNA and Hmga2 protein in NPCs at these stages for embryos infected with the
241 retrovirus for Hmga2 shRNA at E8.0 (Figure 4b and c). We then examined the effect of
242 Hmga2 knockdown on neurogenesis by immunostaining for Tbr2, a marker of
243 intermediate neuronal progenitors and immature neurons (Englund et al., 2005). Whereas
244 Hmga2 knockdown from E8.0 did not affect the fraction of Tbr2-positive cells among
245 GFP-positive cells at E10.0, it significantly attenuated the increase in the fraction of such
246 cells apparent at E11.0 (Figure 4d and e). In contrast, Hmga2 knockdown from E8.0
247 slightly, but not significantly, increased the fraction of cells positive for Sox2, an NPC
248 marker (Ellis et al., 2004), among GFP-positive cells at E11.0 (Figure 4f and g). These
249 results suggested that Hmga2 promotes neurogenesis in neocortical NPCs at the onset of
250 the neurogenic phase. We further examined the role of Hmga2 by transcriptomic analysis.
251 We therefore introduced retroviruses encoding GFP and either control or Hmga2 shRNAs
252 into embryos at E8.0 and isolated GFP-expressing CD133^{high} neocortical NPCs by FACS
253 at E10.0 for RNA-seq analysis, which we performed with the Quartz-seq method for
254 analysis of a small number of cells (Sasagawa et al., 2013) (Figure 5a, b, and
255 Supplementary Figure 2a). The expression of *Hmga2* as well as that of *Igf2bp2*, a target
256 gene of Hmga2 in NPCs (Fujii et al., 2013), were found to be reduced in NPCs of embryos
257 infected with the retrovirus for Hmga2 shRNA (Figure 5b and c), thus confirming the
258 efficient knockdown of Hmga2 by this procedure. Then, we performed gene ontology
259 (GO) analysis with the differentially expressed genes between control and Hmga2-
260 depleted cells at E10.0 and E11.0 determined by the *edgeR* software (Supplementary Data
261 2). We found that the GO of downregulated genes in Hmga2-depleted cells than in control
262 cells included "nervous system development" ($p = 1.1 \times 10^{-2}$, FDR = 0.26 at E10 and $p =$

263 9.3×10^{-4}, FDR = 1.67 at E11) and "generation of neurons" ($p = 9.9 \times 10^{-4}$, FDR = 1.78
264 at E11) (Figure 5d). This also supports the notion that Hmga2 promotes neurogenesis at
265 this early stage.
266 There were at least two possible explanations for the attenuation of
267 neurogenesis by knockdown of Hmga2: Hmga2 might promote the E-to-N transition of
268 NPCs, in which case Hmga2 depletion would be expected to prolong the expansion phase
269 and delay the start of the neurogenic phase; or Hmga2 might promote neuronal
270 differentiation of NPCs during the neurogenic phase without affecting the E-to-N
271 transition of NPCs. To discriminate between these possibilities, we examined whether
272 Hmga2 knockdown might delay the developmental change in the transcriptional profile
273 of neocortical NPCs at the E-to-N transition. We performed gene set enrichment analysis
274 (GSEA) to compare the expression levels of signature genes of NPCs that change from
275 E8.0 to E12.0 between control and Hmga2-depleted NPCs at E10.0. We examined genes
276 in clusters identified in Figure 3 as such signature genes and found that the expression
277 level of genes in cluster 2, which showed the prominent decline from E9.0 to E11.0, was
278 significantly higher (enriched) in Hmga2-depleted NPCs than in control NPCs (Figure 5e,
279 Supplementary Figure 2b-e). This finding suggested that Hmga2 knockdown shifts the
280 transcriptional profile of NPCs closer to that apparent in the expansion phase, providing
281 support for the notion that the observed increase in Hmga2 expression promotes the E-
282 to-N transition of NPC fate in the neocortex. We previously showed that Hmga2
283 knockdown during the late neurogenic phase did not promote premature neuronal
284 differentiation (Kishi et al., 2012), which further supports the notion that Hmga2
285 promotes the E-to-N transition of NPC fate rather than neuronal differentiation of NPCs
286 per se.
287 Of interest, the genes which showed increased expression at both E10.0 and
288 E11.0 by Hmga2 knockdown from E8.0 included *Hist1h2bn*, that encodes histone H2B,
289 and *Mki67*, that encodes Ki67, both of which being related to proliferation
290 (Supplementary Figure 2f). This may suggest a possibility that Hmga2 contributes to
291 some aspects of cell division, although Hmga2 knockdown from E8.0 did not overtly
292 increase the fraction of NPCs positive for phosphorylated histone H3 at E11.0 (data not
293 shown). Together, our results thus implicated Hmga2 in changes in some (including the
294 acquisition of neurogenic potential) but not all properties of NPCs related to this transition.
295

296 **Discussion**

297

298 A directional transition of NPC fate from the expansion phase to the neurogenic phase
299 takes place during the early stage of mammalian brain development, but the cell-intrinsic
300 programs that govern this transition have remained largely unclear. Given that
301 neurogenesis can be observed at least from E10 in the mouse neocortex, we assumed that
302 this E-to-N transition takes place around E10 and identified gene sets that are specifically
303 up- or down-regulated around the time of this transition. Among the highly expressed
304 genes whose expression peaks around this transition, we focused on that for the
305 chromatin-associated protein Hmga2 and examined the effects of its knockdown with the
306 use of a method we developed in this study for the genetic manipulation of early-stage
307 NPCs before neural tube closure. We thus found that forced depletion of Hmga2 in
308 neocortical NPCs from E8.0 hindered the increase in neurogenesis apparent at the onset
309 of the neurogenic phase (from E10.0 to E11.0). Moreover, we found that this effect of
310 Hmga2 depletion was likely due to a delay in the E-to-N transition of NPC fate rather
311 than to inhibition of neuronal differentiation per se within the neurogenic phase, given
312 the delayed change in the transcriptional profile of NPCs induced by the loss of Hmga2.
313 On the basis of our results, we propose that the increase in Hmga2 expression apparent at
314 the E-to-N transition promotes this transition of NPC fate—in particular, by promoting
315 the acquisition of neurogenic potential.

316 Investigation of the molecular mechanism underlying the E-to-N transition of
317 NPC fate in any detail requires manipulation of gene expression before neural tube
318 closure. However, existing (convenient and simple) methods such as injection into the
319 ventricles of viruses or of plasmids for in utero electroporation (Tabata and Nakajima,
320 2001) can be applied only after neural tube closure. The method for gene introduction
321 developed in the present study has several advantages over other methods that can be
322 used before neural tube closure, such as whole-embryo genomic manipulation (gene
323 targeting or transgene introduction) and ultrasound-guided injection of viruses into the
324 mouse nervous system. Whereas genomic manipulation requires a specific Cre-
325 expressing mouse line or knowledge of specific distal elements to control expression of
326 a gene of interest in a temporally and spatially regulated manner, our method allows
327 expression of a gene of interest in NPCs as well as in other ectodermal or endodermal
328 cells before neural tube closure without such mouse lines or knowledge. Our method is

329 also less costly, less labor-intensive, and less time-consuming compared with existing
330 methods and is thus suitable for testing and screening a large number of genes for their
331 specific effects (Gaiano et al., 1999; Mangold et al., 2021). The relatively simple and
332 rapid nature of our procedure also appears to be beneficial in terms of minimizing
333 developmental abnormalities and maximizing the survival rate of manipulated embryos
334 compared with the ultrasound-guided injection of viruses (Gaiano et al., 1999). Given
335 that many recent studies based on brain organoids have implicated various molecules as
336 potential regulators of early brain development, a simple and efficient method for gene
337 introduction into early-stage mouse NPCs would be useful for rapid testing of the
338 functions of these molecules in the in vivo context.

339 Given the proposed function of Hmga2 as a trigger of the E-to-N transition, the
340 timing of the increase in Hmga2 abundance may play an important role in determining
341 that of the E-to-N transition. We indeed found that the amount of *Hmga2* mRNA peaks at
342 around the time of this transition (at ~E10) in mouse neocortical NPCs. Then, what
343 upstream pathways (mechanisms) might regulate this increase of *Hmga2* expression? It
344 is possible that extrinsic factors implicated in the E-to-N transition in the mouse neocortex,
345 such as FGF10 and atRA, contribute to the regulation of *Hmga2* expression. Of note, the
346 promoter of the mouse *Hmga2* gene contains putative retinoic acid–responsive elements
347 that are able to bind retinoic acid receptors (data not shown). Myc proteins as well as the
348 Lin28–*let7* microRNA axis have also been shown to promote the expression of *Hmga2*
349 in other cell types (Chang et al., 2009; Copley et al., 2013; Lee and Dutta, 2007; Mayr et
350 al., 2007). Although we did not detect an increase in the expression of Myc-family
351 proteins around E9 to E11, we found that the level of *Lin28b* mRNA increases in
352 neocortical NPCs before that of *Hmga2* mRNA at around this time of development (data
353 not shown). It will therefore be of interest to examine the relevance of Lin28 to the
354 regulation of *Hmga2* expression in the context of the E-to-N transition in the mouse
355 neocortex.

356 Then, how does Hmga2 regulate the E-to-N transition? Previous reports have
357 shown the regulation of certain genes (such as *CcnA2*, *Igf2bp2*, and *Plag1*) through direct
358 association of Hmga2 with their promoters (Cleynen et al., 2007; Li et al., 2012; Sakai et
359 al., 2019; Tessari et al., 2003; Vignali and Marracci, 2020). To investigate the target genes
360 of Hmga2 during the E-to-N transition, we determined differentially expressed genes
361 between control and Hmga2-depleted NPCs in Figure 5 using the *edgeR* software

362 (Supplementary Data 2). The differentially expressed genes (the genes upregulated by
363 Hmga2 knockdown) included *Igf2bp2*, *Wnt7b* and *Jag1*. *Igf2bp2* is a well-known target
364 of Hmga2 and contributes to the neurogenic potential of NPCs (Fujii et al., 2013). *Wnt7b*
365 is expressed in the developing neocortex (Kim et al., 2001) where the Wnt signaling
366 pathway promotes both neurogenesis and proliferation of NPCs (Chenn and Walsh, 2002;
367 Hirabayashi et al., 2004; Israsena et al., 2004; Muroyama et al., 2004; Woodhead et al.,
368 2006; Wrobel et al., 2007; Zhou et al., 2006). The Notch ligand Jag1 is also expressed in
369 neocortical NPCs (Blackwood, 2019; Cárdenas et al., 2018) where Notch signaling plays
370 a crucial role in the E-to-N transition (Gaiano et al., 2000; Hatakeyama et al., 2004).
371 Importantly, by performing a ChIP-seq analysis of Hmga2 with E11 neocortices, we
372 found deposition of Hmga2 protein peaks around the *Igf2bp2*, *Wnt7b* and *Jag1* gene loci
373 (Supplementary Figure 3). Therefore, Hmga2 may promote the E-to-N transition of NPCs
374 in part by enhancing the expression of these genes. In addition, we found a slight tendency
375 that genes expressed higher at E11.0 by Hgma2 depletion from E8.0 are enriched with
376 genes whose expression is derepressed by deletion of Ring1B (in 9 days in vitro NPC
377 culture from E11) (Hirabayashi et al., 2009) or Ring1A/B (in neocortical NPCs at E18),
378 the central component of Polycomb group proteins (PcG) (Supplementary Figure 4a and
379 b). Given the role of PcG in suppressing neurogenic genes in the developing neocortex
380 (Hirabayashi et al., 2009; Morimoto-Suzki et al., 2014; Pereira et al., 2010; Tsuboi et al.,
381 2018), these results may suggest that Hmga2 positively regulates expression of some
382 neurogenic genes by antagonizing PcG-mediated suppression.
383 The search for the "timer" of the E-to-N transition is especially relevant to our
384 understanding of the evolutionary enlargement of the brain, given that the duration of the
385 expansion phase (or the number of symmetric NPC divisions) is expected to positively
386 correlate with the size of the founder NPC pool. Indeed, the enlargement of the neocortex
387 in primates as compared with rodents appears to be related to lengthening of the
388 expansion phase from a few days to several weeks (Dehay et al., 2015; Kornack and Rakic,
389 1998; Rakic, 1995; Rakic, 2009) in addition to the emergence of additional proliferative
390 NPC populations (such as outer/basal RGCs) (Betizeau et al., 2013; Fietz et al., 2010;
391 Hansen et al., 2010) and the continuation of proliferative NPC divisions even after the
392 onset of neurogenesis (Otani et al., 2016). Even among primates, the cell-autonomous
393 timing of the E-to-N transition in cultured NPCs is delayed in humans compared with
394 nonhuman primates (Otani et al., 2016). Of interest, the level of *HMGA2* mRNA also

395 seems to be high in neocortical NPCs at around the onset of neurogenesis (gestation week
396 7 to 8) during early human development (Nowakowski et al., 2017). Moreover, *HMGA2*
397 was found to be one of the genes that most markedly influence the velocity stream
398 associated with timing of NPC fate transition at the early stage of human neocortical
399 development (Eze et al., 2021), suggesting the possibility that HMGA2 plays a conserved
400 role in the onset of the neurogenic phase in humans. If this is the case, the difference in
401 the regulation of Hmga2 gene expression between mouse and human may provide insight
402 into the timing of this transition.
403 The size of the neocortex is strictly regulated during mammalian development,
404 with disorders that result from defects in such regulation in humans, such as
405 macrocephaly and microcephaly, being associated with pathological or psychiatric
406 conditions such as epilepsy, autism spectrum disorder, and schizophrenia (Sun and
407 Hevner, 2014). A single-cell transcriptomic analysis of human neocortical progenitors
408 indicated that genes that drive the early-stage transition of NPC fate are enriched in those
409 associated with neurodevelopmental or psychiatric disorders (Eze et al., 2021). It will
410 thus be of interest to investigate the impact of Hmga2 and its related molecules on
411 neocortical size and, ultimately, neocortical function.
412
413

414 **Materials and Methods**

415

416 **Mouse maintenance**

417 All animals were studied according to protocols approved by the Animal Care and Use
418 Committee of The University of Tokyo. *Ring1a*$^{-/-}$;*Ring1b*$^{flox/flox}$ mice (Calés et al., 2008;
419 Endoh et al., 2008) were crossed with *Rosa26-CreERT2* mice (Taconic), in which
420 expression of *CreERT2* is driven by the endogenous *Rosa26* promoter. All mice were
421 maintained in a temperature- and relative humidity–controlled (23° ± 3°C and 50 ± 15%,
422 respectively) environment with a normal 12-h-light, 12-h-dark cycle. Two to six mice
423 were housed per sterile cage (Innocage, Innovive; or Micro BARRIER Systems, Edstrom
424 Japan) containing bedding chips (PALSOFT, Oriental Yeast; or PaperClean, SLC Japan),
425 and they were provided with irradiated food (CE-2, CLEA Japan) and filtered water ad
426 libitum. For in utero injection before neural tube closure, mice were allowed to mate for
427 2 h and the female was then checked for a vaginal plug. The time of plug confirmation
428 was defined as E0.0. For induction of CreERT2 activity, pregnant mice were injected
429 intraperitoneally with 150 μl of tamoxifen (Sigma) dissolved in sunflower oil (Nacalai)
430 at a concentration of 10 mg/ml.

431

432 **In utero injection and electroporation before neural tube closure**

433 Jcl:ICR (CLEA Japan) or Slc:ICR (SLC Japan) mice were used for in utero injection
434 experiments. Pregnant mice were injected intraperitoneally with a sodium pentobarbital–
435 based anesthetic, and the uterine horn was exposed and pinched between a flexible fiber-
436 optic cable and a finger (Matsui et al., 2011). Lighting from the fiber-optic cable allowed
437 visualization of the internal uterine structure but did not allow the embryo to be
438 distinguished from the amnion. A small volume (~0.5 μl) of CFSE (1 mM, Sigma),
439 plasmid DNA (1 μg/μl), or retroviruses, each mixed with FastGreen (Chroma
440 Gesellschaft), was injected with a sharpened capillary at an angle perpendicular to the
441 center of the uterus. An injection depth of 1 to 2 mm below the uterine wall allowed the
442 reproducible introduction of the capillary contents into amniotic fluid. For electroporation,
443 the uterus was held between the tweezer-type electrodes (CUY652P2.5x4, Nepa Gene)
444 and electroporated with a NEPA21 system (Nepa Gene) according to the following
445 program: three poring pulses of 30 V with a 15-ms pulse width and 450-ms pulse interval
446 and 10% decay (+ pulse orientation), and two transfer pulses of 10 V with a 50-ms pulse

447 width and 450-ms pulse interval and 10% decay (± pulse orientation). After the injection
448 and electroporation were completed, the uterine horn was placed back into its original
449 location. Embryos were imaged with a fluorescence stereo microscope (2.0× lens, Nikon
450 SMZ18).
451
452 **Plasmid construction**
453 The cDNA for mCherry was cloned by PCR, and its coding sequence was verified by
454 DNA sequencing. The cDNA was subcloned into pCAGEN (a kind gift from C. L. Cepko)
455 to generate the pCAGEN-mCherry plasmid.
456
457 **Retrovirus production and concentration**
458 Retroviruses were produced by transfection of PLAT-GP cells (a kind gift from T.
459 Kitamura) with the previously validated retroviral vectors pSIREN-siLuc (for control
460 shRNA, Addgene #122287) or pSIREN-siHmga2 (for Hmga2 shRNA, Addgene
461 #122290) (Kishi et al., 2012) and with a VSVG plasmid (a kind gift from H. Song).
462 Conditioned medium collected 72 h after the onset of transfection was cleared of debris
463 by centrifugation at 2500 × *g* for 5 min, passed through a 0.45-μm filter, and centrifuged
464 at 250,000 × *g* for 90 min at 4°C and then at 20,000 × *g* for >12 h at 4°C. The resulting
465 virus pellet was suspended in phosphate-buffered saline (PBS). For in utero injection, 10
466 ml of conditioned medium from PLAT-GP cells in a 10-cm dish was concentrated into 10
467 μl of PBS.
468
469 **Flow cytometry and FACS**
470 The telencephalon or neocortex of ICR embryos was dissected and subjected to enzymatic
471 digestion with a papain-based solution (Sumitomo Bakelite). For quantification of the
472 efficiency of gene introduction, the cells were directly subjected to flow cytometric
473 analysis with a FACS Aria instrument (Becton Dickinson). For isolation of NPCs, the
474 cells were stained with allophycocyanin-conjugated antibodies to CD133 (1:400 dilution,
475 BioLegend 141210) and sorted with a FACS Aria instrument (Becton Dickinson). The
476 threshold of CD133 intensity for selection of NPCs was set as follows: E8.0, top 80%;
477 E9.0, top 70%; E10.0, top 60%; E11.0, top 50%; and E12.0, top 50%.
478
479 **Immunohistofluorescence analysis**

480 Immunohistofluorescence staining was performed as previously described (Morimoto-
481 Suzki et al., 2014), with minor modifications including fixation for 3 h without perfusion
482 and the use of a blocking buffer comprising 0.1% Triton X-100 and 3% bovine serum
483 albumin. Primary antibodies and dilutions for immunostaining were as follows: anti-
484 Hmga2, 1:500 (Cell Signaling); anti-Sox2, 1:500 (Cell Signaling); anti-Tbr2, 1:500
485 (chick, Millipore); anti–phospho-histone H3, 1:500 (Cell Signaling); and anti-GFP,
486 1:2000 (Abcam) or 1:1000 (Nakalai). Images were acquired with a laser-scanning
487 confocal microscope (TSC-SP5, Leica) and ImageJ software (NIH). For quantification,
488 the average value of multiple sections of the telencephalon along the rostrocaudal axis
489 was determined for each embryo. We quantified following number of sections and GFP-
490 positive cells. For Figure 4e, 18 or 12 sections for control and 20 or 11 sections for Hmga2
491 KD at E10 or E11, respectively, and 2068 or 1385 cells for control and 3448 or 789, cells
492 for Hmga2 KD at E10 or E11, respectively. For Figure 4g, 10 sections for control and 8
493 sections for Hmga2 KD and 764 cells for control and 493 cells for Hmga2 KD.
494
495 **RT-qPCR analysis**
496 Total RNA was isolated from cells with the use of RNAiso plus (Takara), and up to 0.5
497 μg of the RNA was subjected to RT with the use of ReverTra Ace qPCR RT Master Mix
498 with gDNA remover (Toyobo). The resulting cDNA was subjected to real-time PCR
499 analysis in a LightCycler 480 instrument (Roche) with either KAPA SYBR FAST for
500 LightCycler 480 (Kapa Biosystems) or Thunderbird SYBR qPCR Mix (Toyobo). The
501 amount of each target mRNA was normalized by that of *Actb* mRNA. Primer sequences
502 (5' to 3'; forward and reverse, respectively) were as follows: *Actb*, AATAGT
503 CATTCCAAGTATCCATGAAA and GCGACCATCCTCCTCTTAG; *Hmga2*,
504 CCTGTGAGCCCTCTCCTA and CTTTCTTCTGGGCTGCTT; *Igf2bp2*,
505 CTCTCGGGTAAAGTGGAATTG and CGAATCTGGATTCTTCTGCTC; *Lin28b*,
506 ACCTATGACTCATTGTTGACC and TATCCTGACACTTTCTCGTCG; *GLAST*,
507 CAAGTTCTGCCACCCTAC and CACAAATCTGGTGATGCGT (Sakai et al., 2019).
508
509 **RNA-seq analysis**
510 Libraries for RNA-seq analysis were constructed from total RNA isolated as for RT-qPCR
511 analysis. An Illumina TruSeq RNA sample preparation kit was used for template
512 preparation, which was followed by deep sequencing on the Illumina HiSeq platform to

513 obtain 36-base single-end reads. Approximately 20 million sequences were obtained.
514 Sequenced reads of NPCs isolated from wild-type embryos or from Ring1A/B knockout
515 embryos were mapped to the reference mouse genome mm10 or mm9 with the use of
516 Hisat2 (Kim et al., 2019) or ELAND (Illumina), respectively. Only uniquely mapped and
517 "deduplicated" reads with no base mismatch were used. Expression information was
518 obtained as RPKM based on the RefSeq gene models and with the use of featureCounts
519 (Liao et al., 2014). Gene clustering analysis based on expression patterns was performed
520 with *maSigPro* (Conesa et al., 2006). GO analysis for functional annotation was
521 conducted with DAVID software (Huang et al., 2009).
522
523 **Quartz-seq analysis**
524 Both cDNA synthesis and amplification were performed with total RNA from 1000 cells
525 as described previously (Sasagawa et al., 2013). The amplified cDNA was prepared for
526 sequencing with the use of a Nextera XT DNA Sample Prep Kit (Illumina) and was
527 subjected to deep sequencing analysis on the Illumina HiSeq platform to yield 36-base
528 single-end reads. Approximately 2 million sequences were obtained from each sample.
529 Sequences were mapped to the reference mouse genome (mm10) with Hisat2 (Kim et al.,
530 2019). Only uniquely mapped and "deduplicated" reads with no base mismatch were used.
531 Gene expression was quantitated as RPKM on the basis of RefSeq gene models (mm10)
532 with the use of featureCounts (Liao et al., 2014).
533
534 **GSEA**
535 Enrichment of signature genes was assessed with GSEA software (Subramanian et al.,
536 2005). Each gene set was determined as follows. Expansion-phase genes: genes expressed
537 in cluster 2 at ≥50 RPKM at E9.0. Ring1B target genes in cultured NPCs: Ring1B
538 knockout (KO)/control ≥ 1.5, expression in control ≥ 3.0 RPKM (Hirabayashi et al., 2009).
539 Ring1B target genes in NPCs in vivo: Ring1A/B KO/Ring1A KO ≥ 3.0, expression in
540 control (Ring1A KO) ≥ 1.0 RPKM.
541
542 **ChIP-seq analysis**
543 ChIP analysis was performed as previously described (Sakai et al., 2019) with antibodies
544 to Hmga2 (Cell Signaling). Two million cells directly isolated from the neocortex of
545 embryos at E11.0 were used for ChIP-seq of Hmga2. An Illumina TruSeq DNA sample

546 preparation kit was used for template preparation, which was followed by deep
547 sequencing analysis on the Illumina HiSeq platform to obtain 36-base single-end reads.
548 Sequences were mapped to the reference mouse genome (mm10) with bowtie software
549 (Langmead et al., 2009). Only uniquely mapped reads without blacklist regions
550 determined by the ENCODE project (Amemiya et al., 2019) were used.
551
552 **Statistical analysis**
553 Data presented as means + SEM were compared with the two-tailed Student's paired or
554 Welch's *t* test or by one-way analysis of variance (ANOVA) followed by the Bonferroni-
555 Holm multiple-comparison test. A p value of <0.05 was considered statistically
556 significant.
557
558 **Data availability statement**
559 The sequence data have been deposited in the DNA Data Bank of Japan (DDBJ) Sequence
560 Read Archive under the following IDs: DRA008425 (RNA-seq of WT NPCs),
561 DRA010293 (Quartz-seq of Hmga2 KD NPCs), DRA008363, DRA010295 (Hmga2
562 ChIP-seq) and DRA010297 (H3K27me3 ChIP-seq).
563
564

565 **Acknowledgments**
566 We thank T. Shimogori (RIKEN) as well as M. Miura, Y. Yamaguchi, K. Hashimoto, and
567 H. Miyazawa (The University of Tokyo) for technical advice regarding in utero injection
568 before neural tube closure; I. Nikaido (RIKEN) for advice on Quartz-seq analysis; K.
569 Imamura, T. Horiuchi, and S. Sugano (The University of Tokyo) for assistance with high-
570 throughput sequencing analysis; Y. Koseki (RIKEN) for providing *Ring1* mutant mice; H.
571 Song (Johns Hopkins University School of Medicine, Baltimore, MD) for the plasmid
572 encoding the VSVG; T. Kitamura (The University of Tokyo) for PLAT-GP cells; C. L.
573 Cepko (Harvard Medical School) for the pCAGEN plasmid; The One-Stop Sharing
574 Facility Center for Future Drug Discoveries (The University of Tokyo) for FACS; R.
575 Nagayoshi, and Y. Kakeya (The University of Tokyo) for technical assistance; and
576 members of the Gotoh laboratory for discussion. This research was supported by AMED-
577 CREST (JP20gm1310004 to Y.G.), by AMED-PRIME (JP20gm6110021 to Y.K.), and by
578 MEXT/JSPS KAKENHI (JP16H06481 and JP16H06479 to Y.G.; JP19H05253,
579 JP20H03179, JP20H05383, and JP16H06279 to Y.K.).
580
581 **Author Contributions**
582 N.K., Y.K., Y.H. and Y.G. designed the study and wrote the manuscript. N.K., Y.K., Y.M.,
583 Y.N., and Y.H. performed the experiments and analyzed the data. Y.S. performed high-
584 throughput sequencing analysis. H.K. generated *Ring1a*$^{-/-}$;*Ring1b*$^{flox/flox}$ mice. Y.K., Y.H.,
585 and Y.G. supervised the study.
586
587 **Declaration of Interests**
588 The authors declare no competing interests.
589
590
591

References

Amemiya, H. M., Kundaje, A. and Boyle, A. P. (2019). The ENCODE Blacklist: Identification of Problematic Regions of the Genome. *Scientific reports* **9**, 9354–5.

Anthony, T. E., Mason, H. A., Gridley, T., Fishell, G. and Heintz, N. (2005). Brain lipid-binding protein is a direct target of Notch signaling in radial glial cells. *Genes & Development* **19**, 1028–1033.

Benito-Kwiecinski, S., Giandomenico, S. L., Sutcliffe, M., Riis, E. S., Freire-Pritchett, P., Kelava, I., Wunderlich, S., Martin, U., Wray, G. A., McDole, K., et al. (2021). An early cell shape transition drives evolutionary expansion of the human forebrain. *Cell*.

Betizeau, M., Cortay, V., Patti, D., Pfister, S., Gautier, E., Bellemin-Ménard, A., Afanassieff, M., Huissoud, C., Douglas, R. J., Kennedy, H., et al. (2013). Precursor diversity and complexity of lineage relationships in the outer subventricular zone of the primate. *Neuron* **80**, 442–457.

Blackwood, C. A. (2019). Jagged1 is Essential for Radial Glial Maintenance in the Cortical Proliferative Zone. *Neuroscience* **413**, 230–238.

Calés, C., Roman-Trufero, M., Pavón, L., Serrano, I., Melgar, T., Endoh, M., Pérez, C., Koseki, H. and Vidal, M. (2008). Inactivation of the polycomb group protein Ring1B unveils an antiproliferative role in hematopoietic cell expansion and cooperation with tumorigenesis associated with Ink4a deletion. *Molecular and Cellular Biology* **28**, 1018–1028.

Cárdenas, A., Villalba, A., Romero, C. de J., Picó, E., Kyrousi, C., Tzika, A. C., Tessier-Lavigne, M., Ma, L., Drukker, M., Cappello, S., et al. (2018). Evolution of Cortical Neurogenesis in Amniotes Controlled by Robo Signaling Levels. *Cell* **174**, 590-606.e21.

619 **Chang, T.-C., Zeitels, L. R., Hwang, H.-W., Chivukula, R. R., Wentzel, E. A.,**
620 **Dews, M., Jung, J., Gao, P., Dang, C. V., Beer, M. A., et al.** (2009). Lin-28B
621 transactivation is necessary for Myc-mediated let-7 repression and proliferation.
622 *Proceedings of the National Academy of Sciences* **106**, 3384–3389.

623 **Chau, K. F., Shannon, M. L., Fame, R. M., Fonseca, E., Mullan, H., Johnson, M.**
624 **B., Sendamarai, A. K., Springel, M. W., Laurent, B. and Lehtinen, M. K.** (2018).
625 Downregulation of ribosome biogenesis during early forebrain development. *eLife*
626 **7**,.

627 **Chenn, A. and Walsh, C. A.** (2002). Regulation of Cerebral Cortical Size by Control
628 of Cell Cycle Exit in Neural Precursors. *Science* **297**, 365–369.

629 **Cleynen, I., Brants, J. R., Peeters, K., Deckers, R., Debiec-Rychter, M., Sciot, R.,**
630 **Ven, W. J. M. V. D. and Petit, M. M. R.** (2007). HMGA2 regulates transcription of
631 the Imp2 gene via an intronic regulatory element in cooperation with nuclear factor-
632 kappaB. *Molecular cancer research : MCR* **5**, 363–372.

633 **Conesa, A., Conesa, A., Nueda, M. J., Nueda, M. J., Ferrer, A., Ferrer, A., Talón,**
634 **M. and Talón, M.** (2006). maSigPro: a method to identify significantly differential
635 expression profiles in time-course microarray experiments. *Bioinformatics* **22**, 1096–
636 1102.

637 **Copley, M. R., Babovic, S., Benz, C., Knapp, D. J. H. F., Beer, P. A., Kent, D. G.,**
638 **Wohrer, S., Treloar, D. Q., Day, C., Rowe, K., et al.** (2013). The Lin28b-let-7-
639 Hmga2 axis determines the higher self-renewal potential of fetal haematopoietic
640 stem cells. *Nature Cell Biology*.

641 **Dehay, C., Kennedy, H. and Kosik, K. S.** (2015). The outer subventricular zone and
642 primate-specific cortical complexification. *Neuron* **85**, 683–694.

643 **Eiraku, M., Watanabe, K., Matsuo-Takasaki, M., Kawada, M., Yonemura, S.,**
644 **Matsumura, M., Wataya, T., Nishiyama, A., Muguruma, K. and Sasai, Y.**
645 (2008). Self-organized formation of polarized cortical tissues from ESCs and its
646 active manipulation by extrinsic signals. *Cell Stem Cell* **3**, 519–532.

647 **Ellis, P., Fagan, B. M., Magness, S. T., Hutton, S., Taranova, O., Hayashi, S.,**
648 **McMahon, A., Rao, M. and Pevny, L.** (2004). SOX2, a persistent marker for
649 multipotential neural stem cells derived from embryonic stem cells, the embryo or
650 the adult. *Developmental neuroscience* **26**, 148–165.

651 **Endoh, M., Endo, T. A., Endoh, T., Fujimura, Y.-I., Ohara, O., Toyoda, T., Otte,**
652 **A. P., Okano, M., Brockdorff, N., Vidal, M., et al.** (2008). Polycomb group
653 proteins Ring1A/B are functionally linked to the core transcriptional regulatory
654 circuitry to maintain ES cell identity. *Development* **135**, 1513–1524.

655 **Englund, C., Fink, A., Lau, C., Pham, D., Daza, R. A. M., Bulfone, A., Kowalczyk,**
656 **T. and Hevner, R. F.** (2005). Pax6, Tbr2, and Tbr1 are expressed sequentially by
657 radial glia, intermediate progenitor cells, and postmitotic neurons in developing
658 neocortex. *Journal of Neuroscience* **25**, 247–251.

659 **Eze, U. C., Bhaduri, A., Haeussler, M., Nowakowski, T. J. and Kriegstein, A. R.**
660 (2021). Single-cell atlas of early human brain development highlights heterogeneity
661 of human neuroepithelial cells and early radial glia. *Nature Neuroscience*.

662 **Fietz, S. A., Kelava, I., Vogt, J., Wilsch-Bräuninger, M., Stenzel, D., Fish, J. L.,**
663 **Corbeil, D., Riehn, A., Distler, W., Nitsch, R., et al.** (2010). OSVZ progenitors of
664 human and ferret neocortex are epithelial-like and expand by integrin signaling.
665 *Nature Neuroscience* **13**, 690–699.

666 **Fujii, Y., Kishi, Y. and Gotoh, Y.** (2013). IMP2 regulates differentiation potentials of
667 mouse neocortical neural precursor cells. *Genes to Cells* **18**, 79–89.

668 **Gaiano, N., Kohtz, J. D., Turnbull, D. H. and Fishell, G.** (1999). A method for rapid
669 gain-of-function studies in the mouse embryonic nervous system. *Nature*
670 *Neuroscience* **2**, 812–819.

671 **Gaiano, N., Nye, J. S. and Fishell, G.** (2000). Radial glial identity is promoted by
672 Notch1 signaling in the murine forebrain. *Neuron* **26**, 395–404.

673 **Gao, P., Postiglione, M. P., Krieger, T. G., Hernandez, L., Wang, C., Han, Z.,**
674 **Streicher, C., Papusheva, E., Insolera, R., Chugh, K., et al.** (2014). Deterministic
675 progenitor behavior and unitary production of neurons in the neocortex. *Cell* **159**,
676 775–788.

677 **Gaspard, N., Bouschet, T., Hourez, R., Dimidschstein, J., Naeije, G., Ameele, J.**
678 **van den, Espuny-Camacho, I., Herpoel, A., Passante, L., Schiffmann, S. N., et**
679 **al.** (2008). An intrinsic mechanism of corticogenesis from embryonic stem cells.
680 *Nature* **455**, 351–357.

681 **Gotz, M. and Huttner, W. B.** (2005). The cell biology of neurogenesis. *Nature*
682 *Reviews Molecular Cell Biology* **6**, 777–788.

683 **Hansen, D. V., Lui, J. H., Parker, P. R. L. and Kriegstein, A. R.** (2010). Neurogenic
684 radial glia in the outer subventricular zone of human neocortex. *Nature* **464**, 554–
685 561.

686 **Hartfuss, E., Galli, R., Heins, N. and Götz, M.** (2001). Characterization of CNS
687 precursor subtypes and radial glia. *Developmental Biology* **229**, 15–30.

688 **Hatakeyama, J., Bessho, Y., Katoh, K., Ookawara, S., Fujioka, M., Guillemot, F.**
689 **and Kageyama, R.** (2004). Hes genes regulate size, shape and histogenesis of the
690 nervous system by control of the timing of neural stem cell differentiation.
691 *Development* **131**, 5539–5550.

692 **Hirabayashi, Y. and Gotoh, Y.** (2010). Epigenetic control of neural precursor cell fate
693 during development. *Nature Reviews Neuroscience* **11**, 377–388.

694 **Hirabayashi, Y., Itoh, Y., Tabata, H., Nakajima, K., Akiyama, T., Masuyama, N.**
695 **and Gotoh, Y.** (2004). The Wnt/beta-catenin pathway directs neuronal
696 differentiation of cortical neural precursor cells. *Development* **131**, 2791–2801.

697 **Hirabayashi, Y., Suzki, N., Tsuboi, M., Endo, T. A., Toyoda, T., Shinga, J., Koseki,**
698 **H., Vidal, M. and Gotoh, Y.** (2009). Polycomb limits the neurogenic competence of
699 neural precursor cells to promote astrogenic fate transition. *Neuron* **63**, 600–613.

700 **Huang, D. W., Sherman, B. T. and Lempicki, R. A.** (2009). Bioinformatics
701 enrichment tools: paths toward the comprehensive functional analysis of large gene
702 lists. *Nucleic Acids Research* **37**, 1–13.

703 **Israsena, N., Hu, M., Fu, W., Kan, L. and Kessler, J. A.** (2004). The presence of
704 FGF2 signaling determines whether beta-catenin exerts effects on proliferation or
705 neuronal differentiation of neural stem cells. *Developmental Biology* **268**, 220–231.

706 **Kim, A. S., Anderson, S. A., Rubenstein, J. L., Lowenstein, D. H. and Pleasure, S.**
707 **J.** (2001). Pax-6 regulates expression of SFRP-2 and Wnt-7b in the developing CNS.
708 *Journal of Neuroscience* **21**, RC132–RC132.

709 **Kim, D., Paggi, J. M., Park, C., Bennett, C. and Salzberg, S. L.** (2019). Graph-based
710 genome alignment and genotyping with HISAT2 and HISAT-genotype. *Nature*
711 *Biotechnology* **37**, 907–915.

712 **Kishi, Y. and Gotoh, Y.** (2018). Regulation of Chromatin Structure During Neural
713 Development. *Frontiers in neuroscience* **12**, 874.

714 **Kishi, Y., Fujii, Y., Hirabayashi, Y. and Gotoh, Y.** (2012). HMGA regulates the
715 global chromatin state and neurogenic potential in neocortical precursor cells. *Nature*
716 *Neuroscience* **15**, 1127–1133.

717 **Kornack, D. R. and Rakic, P.** (1998). Changes in cell-cycle kinetics during the
718 development and evolution of primate neocortex. *Proceedings of the National*
719 *Academy of Sciences of the United States of America* **95**, 1242–1246.

720 **Kriegstein, A. and Alvarez-Buylla, A.** (2009). The Glial Nature of Embryonic and
721 Adult Neural Stem Cells. *Annual Review of Neuroscience* **32**, 149–184.

722 **Lange, C., Garcia, M. T., Decimo, I., Bifari, F., Eelen, G., Quaegebeur, A., Boon,**
723 **R., Zhao, H., Boeckx, B., Chang, J., et al.** (2016). Relief of hypoxia by
724 angiogenesis promotes neural stem cell differentiation by targeting glycolysis. *The*
725 *EMBO Journal* **35**, 924–941.

726 **Langmead, B., Trapnell, C., Pop, M. and Salzberg, S. L.** (2009). Ultrafast and
727 memory-efficient alignment of short DNA sequences to the human genome. *Genome*
728 *Biology* **10**, R25-10.

729 **Lee, Y. S. and Dutta, A.** (2007). The tumor suppressor microRNA let-7 represses the
730 HMGA2 oncogene. *Genes & Development* **21**, 1025–1030.

731 **Li, Z., Gilbert, J. A., Zhang, Y., Zhang, M., Qiu, Q., Ramanujan, K., Shavlakadze,**
732 **T., Eash, J. K., Scaramozza, A., Goddeeris, M. M., et al.** (2012). An HMGA2-
733 IGF2BP2 axis regulates myoblast proliferation and myogenesis. *Developmental Cell*
734 **23**, 1176–1188.

735 **Liao, Y., Smyth, G. K. and Shi, W.** (2014). featureCounts: an efficient general
736 purpose program for assigning sequence reads to genomic features. *Bioinformatics*
737 **30**, 923–930.

738 **Mangold, K., Mašek, J., He, J., Lendahl, U., Fuchs, E. and Andersson, E. R.** (2021).
739 Highly efficient manipulation of nervous system gene expression with NEPTUNE.
740 *Cell Reports Methods* 100043.

741 **Matsui, A., Yoshida, A. C., Kubota, M., Ogawa, M. and Shimogori, T.** (2011).
742 Mouse in utero electroporation: controlled spatiotemporal gene transfection. *Journal*
743 *of visualized experiments : JoVE*.

744 **Mayr, C., Hemann, M. T. and Bartel, D. P.** (2007). Disrupting the pairing between
745 let-7 and Hmga2 enhances oncogenic transformation. *Science* **315**, 1576–1579.

746 **McLone, D. G. and Bondareff, W.** (1975). Developmental morphology of the
747 subarachnoid space and contiguous structures in the mouse. *The American journal of*
748 *anatomy* **142**, 273–293.

749 **Miyata, T., Kawaguchi, A., Saito, K., Kuramochi, H. and Ogawa, M.** (2002).
750 Visualization of cell cycling by an improvement in slice culture methods. *Journal of*
751 *Neuroscience Research* **69**, 861–868.

752 **Morimoto-Suzki, N., Hirabayashi, Y., Tyssowski, K., Shinga, J., Vidal, M., Koseki,**
753 **H. and Gotoh, Y.** (2014). The polycomb component Ring1B regulates the timed
754 termination of subcerebral projection neuron production during mouse neocortical
755 development. *Development* **141**, 4343–4353.

756 **Mukhtar, T. and Taylor, V.** (2018). Untangling Cortical Complexity During
757 Development. *Journal of experimental neuroscience* **12**, 1179069518759332.

758 **Muroyama, Y., Kondoh, H. and Takada, S.** (2004). Wnt proteins promote neuronal
759 differentiation in neural stem cell culture. *Biochem Bioph Res Co* **313**, 915–921.

760 **Nakagawa, T., Wada, Y., Katada, S. and Kishi, Y.** (2020). Epigenetic regulation for
761 acquiring glial identity by neural stem cells during cortical development. *Glia* **68**,
762 1554–1567.

763 **Nguyen, H., Kerimoglu, C., Pirouz, M., Pham, L., Kiszka, K. A., Sokpor, G., Sakib,**
764 **M. S., Rosenbusch, J., Teichmann, U., Seong, R. H., et al.** (2018). Epigenetic
765 Regulation by BAF Complexes Limits Neural Stem Cell Proliferation by
766 Suppressing Wnt Signaling in Late Embryonic Development. *Stem cell reports*.

767 **Nishino, J., Kim, I., Chada, K. and Morrison, S. J.** (2008). Hmga2 Promotes Neural
768 Stem Cell Self-Renewal in Young but Not Old Mice by Reducing p16Ink4a and
769 p19Arf Expression. *Cell* **135**, 227–239.

770 **Noctor, S. C., Flint, A. C., Weissman, T. A., Dammerman, R. S. and Kriegstein, A.**
771 **R.** (2001). Neurons derived from radial glial cells establish radial units in neocortex.
772 *Nature* **409**, 714–720.

773 **Nowakowski, T. J., Bhaduri, A., Pollen, A. A., Alvarado, B., Mostajo-Radji, M. A.,**
774 **Lullo, E. D., Haeussler, M., Sandoval-Espinosa, C., Liu, S. J., Velmeshev, D., et**
775 **al.** (2017). Spatiotemporal gene expression trajectories reveal developmental
776 hierarchies of the human cortex. *Science* **358**, 1318–1323.

777 **Otani, T., Marchetto, M. C., Gage, F. H., Simons, B. D. and Livesey, F. J.** (2016).
778 2D and 3D Stem Cell Models of Primate Cortical Development Identify Species-

Specific Differences in Progenitor Behavior Contributing to Brain Size. *Cell Stem Cell* **18**, 467–480.

Pereira, J. D., Sansom, S. N., Smith, J., Dobenecker, M.-W., Tarakhovsky, A. and Livesey, F. J. (2010). Ezh2, the histone methyltransferase of PRC2, regulates the balance between self-renewal and differentiation in the cerebral cortex. *Proceedings of the National Academy of Sciences* **107**, 15957–15962.

Qian, X., Goderie, S. K., Shen, Q., Stern, J. H. and Temple, S. (1998). Intrinsic programs of patterned cell lineages in isolated vertebrate CNS ventricular zone cells. *Development* **125**, 3143–3152.

Quah, B. J. C. and Parish, C. R. (2010). The use of carboxyfluorescein diacetate succinimidyl ester (CFSE) to monitor lymphocyte proliferation. *Journal of visualized experiments : JoVE*.

Rakic, P. (1972). Mode of cell migration to the superficial layers of fetal monkey neocortex. *The Journal of Comparative Neurology* **145**, 61–83.

Rakic, P. (1995). A small step for the cell, a giant leap for mankind: a hypothesis of neocortical expansion during evolution. *Trends in Neurosciences* **18**, 383–388.

Rakic, P. (2009). Evolution of the neocortex: a perspective from developmental biology. *Nature Reviews Neuroscience* **10**, 724–735.

Sahara, S. and O'Leary, D. D. M. (2009). Fgf10 regulates transition period of cortical stem cell differentiation to radial glia controlling generation of neurons and basal progenitors. *Neuron* **63**, 48–62.

Sakai, H., Fujii, Y., Kuwayama, N., Kawaji, K., Gotoh, Y. and Kishi, Y. (2019). Plag1 regulates neuronal gene expression and neuronal differentiation of neocortical neural progenitor cells. *Genes to Cells* **24**, 650–666.

Sanosaka, T., Namihira, M., Asano, H., KOHYAMA, J., Aisaki, K., Igarashi, K., Kanno, J. and Nakashima, K. (2008). Identification of genes that restrict astrocyte differentiation of midgestational neural precursor cells. *Neuroscience* **155**, 780–788.

Sasagawa, Y., Nikaido, I., Hayashi, T., Danno, H., Uno, K. D., Imai, T. and Ueda, H. R. (2013). Quartz-Seq: a highly reproducible and sensitive single-cell RNA sequencing method, reveals non-genetic gene-expression heterogeneity. *Genome Biology* **14**, R31.

Shen, Q., Wang, Y., Dimos, J. T., Fasano, C. A., Phoenix, T. N., Lemischka, I. R., Ivanova, N. B., Stifani, S., Morrisey, E. E. and Temple, S. (2006). The timing of cortical neurogenesis is encoded within lineages of individual progenitor cells. *Nature Neuroscience* **9**, 743–751.

Shi, Y., Kirwan, P., Smith, J., Robinson, H. P. C. and Livesey, F. J. (2012). Human cerebral cortex development from pluripotent stem cells to functional excitatory synapses. *Nature Neuroscience* **15**, 477-86-S1.

Siegenthaler, J. A., Ashique, A. M., Zarbalis, K., Patterson, K. P., Hecht, J. H., Kane, M. A., Folias, A. E., Choe, Y., May, S. R., Kume, T., et al. (2009). Retinoic Acid from the Meninges Regulates Cortical Neuron Generation. *Cell* **139**, 597–609.

Subramanian, A., Tamayo, P., Mootha, V. K., Mukherjee, S., Ebert, B. L., Gillette, M. A., Paulovich, A., Pomeroy, S. L., Golub, T. R., Lander, E. S., et al. (2005). Gene set enrichment analysis: A knowledge-based approach for interpreting genome-wide expression profiles. *Proceedings of the National Academy of Sciences of the United States of America* **102**, 15545–15550.

Sun, T. and Hevner, R. F. (2014). Growth and folding of the mammalian cerebral cortex: from molecules to malformations. *Nature Reviews Neuroscience* **15**, 217–232.

Tabata, H. and Nakajima, K. (2001). Efficient in utero gene transfer system to the developing mouse brain using electroporation: visualization of neuronal migration in the developing cortex. *Neuroscience* **103**, 865–872.

831 **Telley, L., Govindan, S., Prados, J., Stévant, I., Nef, S., Dermitzakis, E., Dayer, A.**
832 **and Jabaudon, D.** (2016). Sequential transcriptional waves direct the differentiation
833 of newborn neurons in the mouse neocortex. *Science* **351**, 1443–1446.

834 **Tessari, M. A., Gostissa, M., Altamura, S., Sgarra, R., Rustighi, A., Salvagno, C.,**
835 **Caretti, G., Imbriano, C., Mantovani, R., Sal, G. D., et al.** (2003). Transcriptional
836 activation of the cyclin A gene by the architectural transcription factor HMGA2.
837 *Molecular and Cellular Biology* **23**, 9104–9116.

838 **Tochitani, S., Furukawa, T., Bando, R., Kondo, S., Ito, T., Matsushima, Y.,**
839 **Kojima, T., Matsuzaki, H. and Fukuda, A.** (2021). GABAA Receptors and
840 Maternally Derived Taurine Regulate the Temporal Specification of Progenitors of
841 Excitatory Glutamatergic Neurons in the Mouse Developing Cortex. *Cereb Cortex*.

842 **Tsuboi, M., Kishi, Y., Yokozeki, W., Koseki, H., Hirabayashi, Y. and Gotoh, Y.**
843 (2018). Ubiquitination-Independent Repression of PRC1 Targets during Neuronal
844 Fate Restriction in the Developing Mouse Neocortex. *Developmental Cell* **47**, 758-
845 772.e5.

846 **Tsuboi, M., Hirabayashi, Y. and Gotoh, Y.** (2019). Diverse gene regulatory
847 mechanisms mediated by Polycomb group proteins during neural development.
848 *Current Opinion in Neurobiology* **59**, 164–173.

849 **Vignali, R. and Marracci, S.** (2020). HMGA Genes and Proteins in Development and
850 Evolution. *International Journal of Molecular Sciences* **21**, 654–39.

851 **Woodhead, G. J., Mutch, C. A., Olson, E. C. and Chenn, A.** (2006). Cell-
852 Autonomous β-Catenin Signaling Regulates Cortical Precursor Proliferation. *J*
853 *Neurosci* **26**, 12620–12630.

854 **Wrobel, C. N., Mutch, C. A., Swaminathan, S., Taketo, M. M. and Chenn, A.**
855 (2007). Persistent expression of stabilized β-catenin delays maturation of radial glial
856 cells into intermediate progenitors. *Dev Biol* **309**, 285–297.

857 **Yoon, K., Nery, S., Rutlin, M. L., Radtke, F., Fishell, G. and Gaiano, N.** (2004).
858 Fibroblast growth factor receptor signaling promotes radial glial identity and
859 interacts with Notch1 signaling in telencephalic progenitors. *Journal of*
860 *Neuroscience* **24**, 9497–9506.

861 **Yoon, K.-J., Ringeling, F. R., Vissers, C., Jacob, F., Pokrass, M., Jimenez-Cyrus,**
862 **D., Su, Y., Kim, N.-S., Zhu, Y., Zheng, L., et al.** (2017). Temporal Control of
863 Mammalian Cortical Neurogenesis by m(6)A Methylation. *Cell* **171**, 877-889.e17.

864 **Zahr, S. K., Yang, G., Kazan, H., Borrett, M. J., Yuzwa, S. A., Voronova, A.,**
865 **Kaplan, D. R. and Miller, F. D.** (2018). A Translational Repression Complex in
866 Developing Mammalian Neural Stem Cells that Regulates Neuronal Specification.
867 *Neuron* **97**, 520-537.e6.

868 **Zhang, X., Chen, M. H., Wu, X., Kodani, A., Fan, J., Doan, R., Ozawa, M., Ma, J.,**
869 **Yoshida, N., Reiter, J. F., et al.** (2016). Cell-Type-Specific Alternative Splicing
870 Governs Cell Fate in the Developing Cerebral Cortex. *Cell* **166**, 1147-1162.e15.

871 **Zhou, C. J., Borello, U., Rubenstein, J. L. R. and Pleasure, S. J.** (2006). Neuronal
872 production and precursor proliferation defects in the neocortex of mice with loss of
873 function in the canonical Wnt signaling pathway. *Neuroscience* **142**, 1119–1131.

874
875
876

877 **Figure Legends**

878

879 **Figure 1. In utero injection of mouse embryos before neural tube closure.** (**a** and **b**)
880 The uterine horn of an anesthetized pregnant mouse was exposed at E7.0 or E8.0. (**c** and
881 **d**) The uterus was pinched between an optical fiber and finger (**c**) for injection via a
882 sharpened glass capillary of a solution colored with a dye (FastGreen) and containing
883 either CFSE, a retrovirus, or a plasmid (**d**). (**e**) Embryos at E7.0 (left) or E8.0 (right) were
884 injected with CFSE, dissected out from the uterus at E9.0 or E11.0, respectively, and fixed
885 for visualization of CFSE fluorescence with a fluorescence stereo microscope. Scale bars,
886 0.5 mm (left) or 1 mm (right). (**f**) The survival and labeling rates after in utero introduction
887 of CFSE into mouse embryos as in (**e**).

888

889 **Figure 2. In utero gene introduction by retroviral infection in embryos before neural**
890 **tube closure.** (**a**) Mouse embryos in the same uterus were injected or not with a retrovirus
891 encoding GFP together with an shRNA targeted to luciferase mRNA at E8.0. The embryos
892 were dissected out from the uterus at E11.0, fixed, and examined for GFP fluorescence
893 with a fluorescence stereo microscope. The posterior half of the control embryo was
894 excised for the purpose of identification. Scale bars, 1 mm. (**b**) An embryo at E7.0 was
895 injected as in (**a**) and examined for GFP fluorescence at E11.0. Scale bar, 1 mm. (**c**)
896 Survival rate and labeling rate for embryos injected as in (**a**) and (**b**). (**d**) Flow cytometric
897 analysis of the efficiency of gene introduction. Neocortical cells dissociated from E12.0
898 embryos that had been injected with a retrovirus for GFP at E8.0 were subjected to flow
899 cytometric analysis of GFP expression. (**e**) A sagittal section of an E10.0 embryo injected
900 at E8.0 as in (**a**) was subjected to immunohistofluorescence staining with antibodies to
901 GFP. Nuclei were counterstained with Hoechst 33342. Representative infected tissues are
902 indicated. Scale bar, 1 mm. (**f** and **g**) Higher magnification images of the bronchus (**f**) and
903 spinal cord (**g**) in the section shown in (**e**). Scale bars, 100 μm. (**h**) Embryos at E7.0 (left)
904 or E8.0 (right) were injected with a plasmid for mCherry and subjected to in utero
905 electroporation. They were dissected out from the uterus at E9.0 or E10.0, respectively,
906 fixed, and examined for mCherry fluorescence with a fluorescence stereo microscope.
907 Scale bars, 0.5 mm (left) or 1 mm (right). (**i**) The survival and labeling rates after in utero
908 electroporation of embryos as in (**h**).

909

910 **Figure 3. Hierarchical clustering of differentially expressed genes in NPCs at early**
911 **developmental stages.** (**a**) CD133^{high} cells were isolated as NPCs from the telencephalon
912 at E8.0 and E9.0 and from the neocortex at E10.0, E11.0, and E12.0 by FACS and were
913 subjected to RNA-seq analysis. (**b–f**) Differentially expressed genes in NPCs at the
914 various developmental stages isolated as in (**a**) were categorized into five clusters
915 (clusters 1–5) on the basis of the pattern of expression changes with the use of hierarchical
916 clustering analysis. The expression levels of the genes in each gene cluster are shown as
917 box plots, with the boxes representing the median and upper and lower quartiles and the
918 whiskers indicating the range (left). Enriched GO terms and their *p* values determined by
919 functional annotation of each gene cluster with DAVID software are also shown (right).
920 RPKM, reads per kilobase of mRNA per million total reads. (**g**) The five genes expressed
921 at the highest levels in cluster 5 at E10.0. (**h**) NPCs isolated as in (**a**) from embryos at
922 E9.0, E10.0, E11.0, and E12.0 were subjected to RT-qPCR analysis of *Hmga2* mRNA.
923 Data were normalized by *Actb* mRNA abundance and are means + SEM from five
924 independent experiments. $*p < 0.05$, $**p < 0.01$ (one-way ANOVA followed by the
925 Bonferroni-Holm multiple-comparison test).
926
927 **Figure 4. Hmga2 promotes the onset of neurogenesis in the mouse neocortex.** (**a**)
928 Mouse embryos at E8.0 were subjected to in utero infection with retroviruses encoding
929 GFP and either control or Hmga2 shRNAs, and the brain was isolated from the embryos
930 at E10.0 or E11.0 for isolation of CD133^{high}, GFP^{+} NPCs by FACS. (**b**) NPCs isolated
931 from control and Hmga2–knockdown (KD) embryos as in (**a**) were subjected to RT-qPCR
932 analysis of *Hmga2* mRNA. Data are expressed relative to the corresponding control value
933 and are means + SEM from five independent experiments. $*p < 0.05$, $**p < 0.01$ versus
934 corresponding control value (two-tailed Student's paired *t* test). (**c–g**) The brain of
935 embryos treated as in (**a**) was subjected to immunohistofluorescence analysis with
936 antibodies to GFP and to Hmga2 at E10.0 (**c**), with those to GFP and to Tbr2 at E11.0 (**d**),
937 and with those to GFP and to Sox2 at E11.0 (**f**). Nuclei were counterstained with Hoechst
938 33342. Scale bars, 20 μm (**c**) or 50 μm (**d** and **f**). Arrowheads indicate GFP^{+} cells (**c**). The
939 percentages of Tbr2^{+} cells at E10.0 or E11.0 (**e**) or of Sox2^{+} cells at E11.0 (**g**) among GFP^{+}
940 cells were also determined. Data are means + SEM from six (Tbr2) or three (Sox2)
941 independent experiments (total of 12 control and nine Hmga2-knockdown embryos for

942 Tbr2, and eight control and seven Hmga2-knockdown embryos for Sox2). *$p < 0.05$
943 versus corresponding control value (two-tailed Welch's *t* test).
944
945 **Figure 5. Hmga2 promotes the change in transcriptional profile of NPCs at the E-**
946 **to-N transition.** (**a**) Embryos were subjected to in utero infection with retroviruses
947 encoding GFP and either control or Hmga2 shRNAs at E8.0, and the brain was isolated
948 at E10.0 or E11.0 for isolation of GFP^{+}, $CD133^{high}$ NPCs by FACS and subsequent RNA
949 (Quartz)-seq analysis. Three or four independent experiments were performed with cells
950 isolated at E10.0 or E11.0, respectively. (**b**) A scatter plot shows the expression levels of
951 *Hmga2* and *Igf2bp2* (red dots) as well as other genes (gray dots) indicated as expression
952 lavels (RPKM) in control and Hmga2–knockdown (KD) NPCs. (**c**) Expression levels
953 (RPKM) of *Hmga2* and *Igf2bp2* in control and Hmga2 KD NPCs were determined. Data
954 are means + SEM and are expressed relative to the corresponding control value. *$p < 0.05$,
955 **$p < 0.01$ versus corresponding control value (two-tailed Student's paired *t* test). (**d**)
956 Enriched GO terms among genes downregulated and upregulated by Hmga2 KD were
957 determined by GO analysis. *p* values were determined with DAVID Bioinformatic
958 Resources. (**e**) The Quartz-seq data for control and Hmga2 KD NPCs isolated at E10.0 as
959 in (**a**) were subjected to GSEA for signature genes of the expansion phase (those in cluster
960 2 with an RPKM of ≥50 at E9.0) (Figure 3c). The family-wise error rate (FWER) *p* value
961 and false discovery rate (FDR) *q* value are shown.
962

963 **Supplementary figure legends**

964

965 **Supplementary Figure 1. Expression levels of *Lin28b* and *GLAST* in NPCs from**
966 **E9.0 to E12.0.** (**a**) CD133^{high} cells were isolated as NPCs from the telencephalon at E9.0
967 and from the neocortex at E10.0, E11.0, and E12.0 by FACS as in Figure 3 and were
968 subjected to RT-qPCR analysis for *Lin28b* and *GLAST* mRNAs. Data were normalized
969 by *Actb* mRNA abundance and are means + SEM from five independent experiments.

970

971 **Supplementary Figure 2. The effects of Hmga2 knockdown in NPCs on gene**
972 **expression patterns** (**a**) Sorting strategy of control and Hmga2 KD NPCs in Figure 5.
973 Left panels, distribution GFP signals of cells obtained from the GFP-introduced
974 neocortices; right panels: distribution of CD133 signals of GFP-positive and -negative
975 cells. (**b**–**e**) The Quartz-seq data for control and Hmga2 KD NPCs isolated at E10.0 as in
976 Figure 5 were subjected to GSEA for the gene sets of clusters 1, 3, 4, and 5 in Figure 3b
977 and 3d–f. The family-wise error rate (FWER) *p* value and false discovery rate (FDR) *q*
978 value are shown. (**f**) The list for upregulated genes by Hmga2 knockdown in NPCs both
979 at E10.0 and E11.0 determined by *edgeR* software are shown.

980

981 **Supplementary Figure 3. Hmga2 deposition at the *Igf2bp2*, *Wnt7b*, and *Lef1* gene**
982 **loci.** (**a**–**c**) Neocortical cells at E11 were subjected to ChIP-seq analysis with antibodies
983 to Hmga2. The Hmga2 signals around the *Igf2bp2* (**a**), *Wnt7b* (**b**), and *Lef1* (**c**) gene loci
984 of two representative results from four independent experiments are shown.

985

986 **Supplementary Figure 4. Hmga2 knockdown increases the expression of PcG target**
987 **genes in NPCs.** (**a**) The Quartz-seq data for control and Hmga2 KD NPCs at E11.0 in
988 Figure 5 were subjected to GSEA of PcG target genes previously identified by Ring1B
989 knockout (KO) in an NPC culture (Hirabayashi et al., 2009). The FWER *p* value and FDR
990 *q* value are shown. (**b**) The Quartz-seq data for NPCs at E11.0 in Figure 5 were subjected
991 to GSEA of PcG target genes that we identified by RNA-seq analysis of NPCs isolated
992 by FACS at E18 from the neocortex of *Ring1a*$^{-/-}$;*Ring1b*$^{flox/flox}$;*Rosa-CreERT2*$^{-/-\ or\ +/-}$
993 mouse embryos that had been treated with tamoxifen at E15 (see Materials and Methods).
994 The FWER *p* value and FDR *q* value are shown.

995

Fig. 1

a

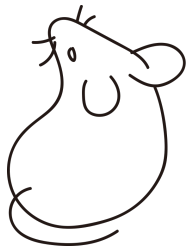

Anesthetized pregnant mouse (E7.0 or E8.0)

b

Exposed uterine horn

c

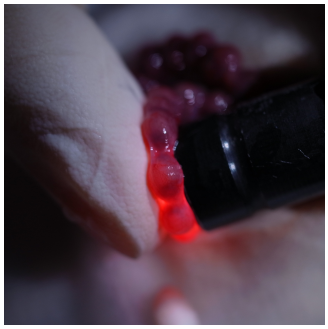

A uterus pinched between an optical fiber and finger

d

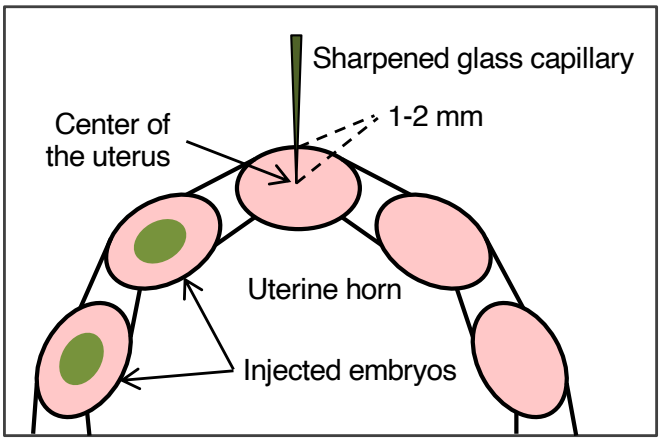

Injection of CFSE, retroviruses, or plasmids

e

E7.0 injection → E9.0

E8.0 injection → E11.0

CFSE

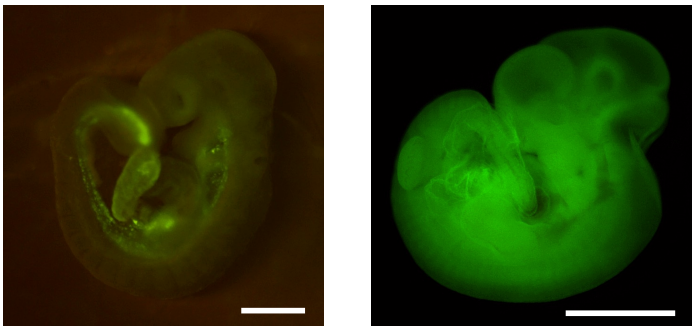

f

	Injected embryos	Survival rate (% of injected)	CFSE-positive (% of injected)
E7.0 injection → E9.0	28	25 (89%)	18 (64%)
E8.0 injection → E10.0	30	24 (80%)	23 (77%)

Fig. 2

a

E8.0 injection → E11.0

Control (no injection) | GFP-expressing virus

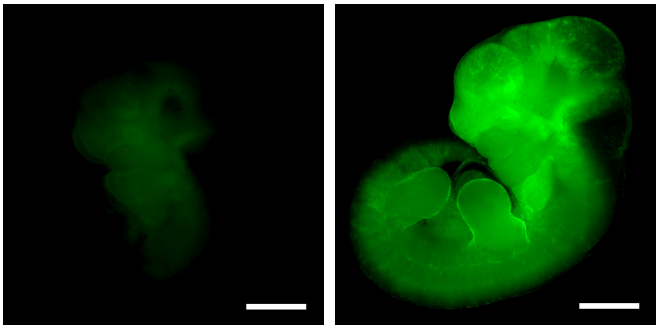

b

E7.0 injection → E11.0

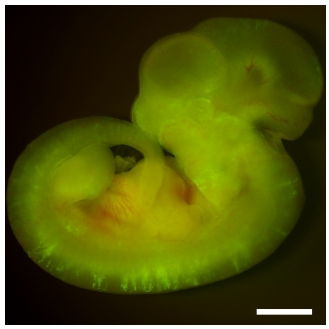

c

	Injected embryos	Survival rate (% of injected)	GFP-positive (% of injected)
E7.0 injection → E9.0	28	27 (96%)	2 (7%)
E8.0 injection → E10.0	19	17 (89%)	14 (74%)

d

E8.0 injection → E12.0

Control (no injection)

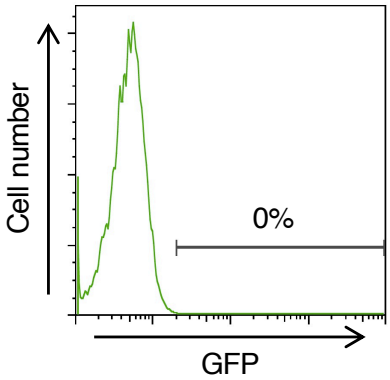

GFP-expressing virus

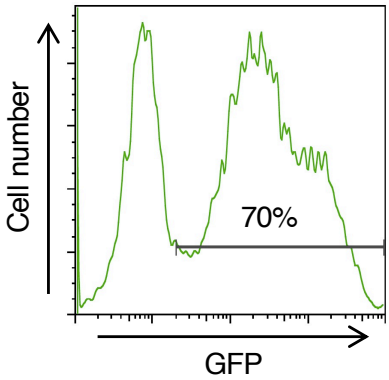

e

E8.0 injection → E10.0

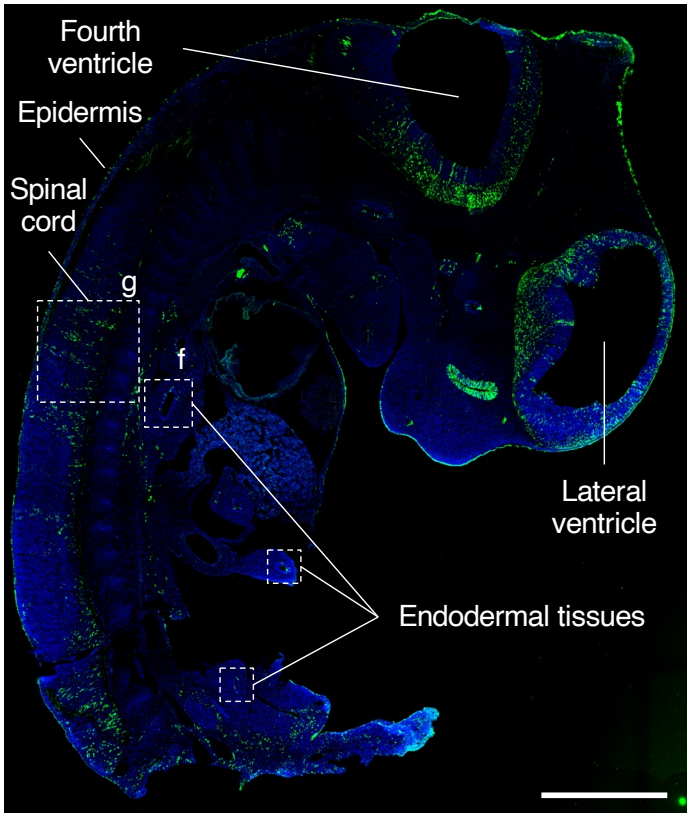

f

Bronchus

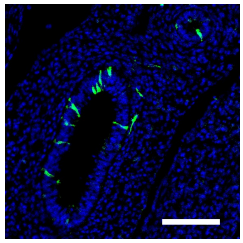

g

Spinal cord

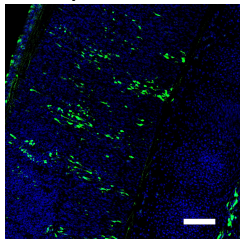

h

E7.0 IUE → E9.0 | E8.0 IUE → E10.0

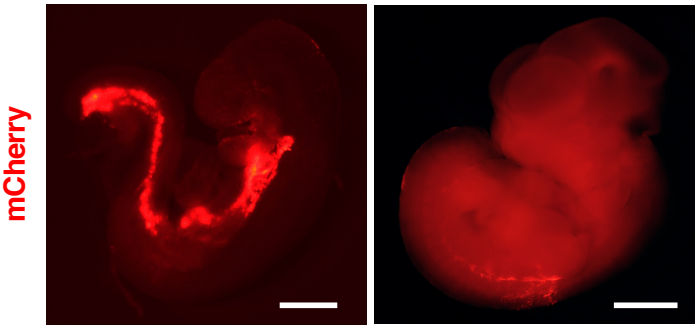

i

	Injected embryos	Survival rate (% of injected)	mCherry-positive (% of injected)
E7.0 → E9.0	36	26 (72%)	7 (19%)
E8.0 → E10.0	20	11 (55%)	8 (40%)

Fig. 3

a

E8.0 whole brain
E9.0 whole brain
E10.0 neocortex
E11.0 neocortex
E12.0 neocortex

→ FACS (CD133^{high}), RNA-seq

b

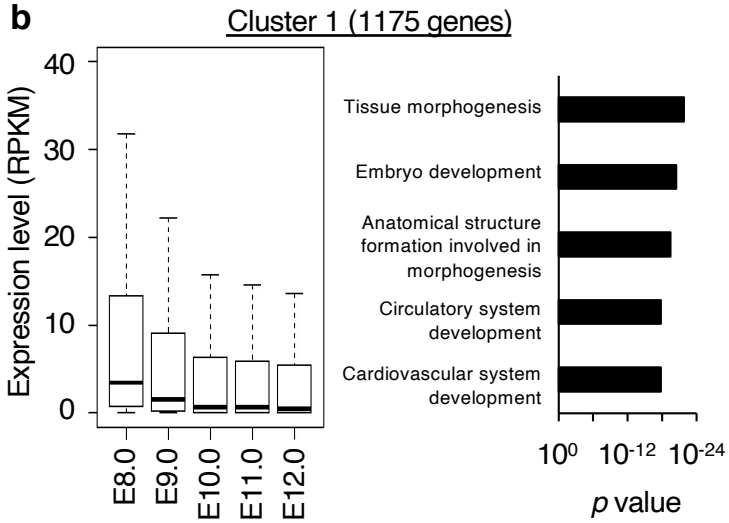

c

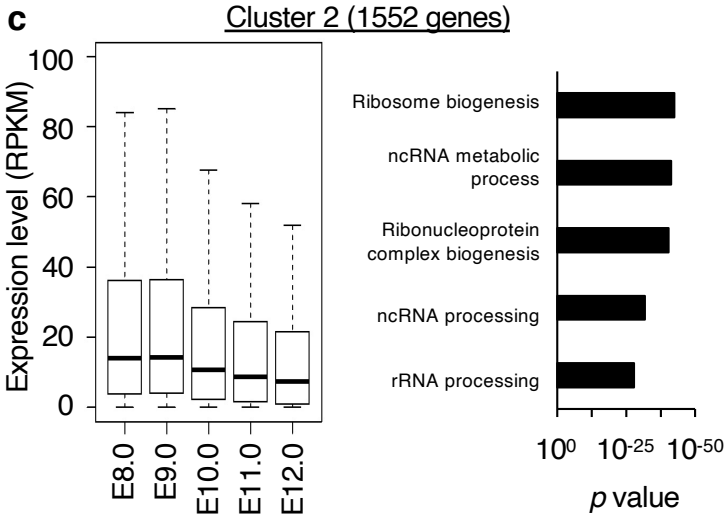

d

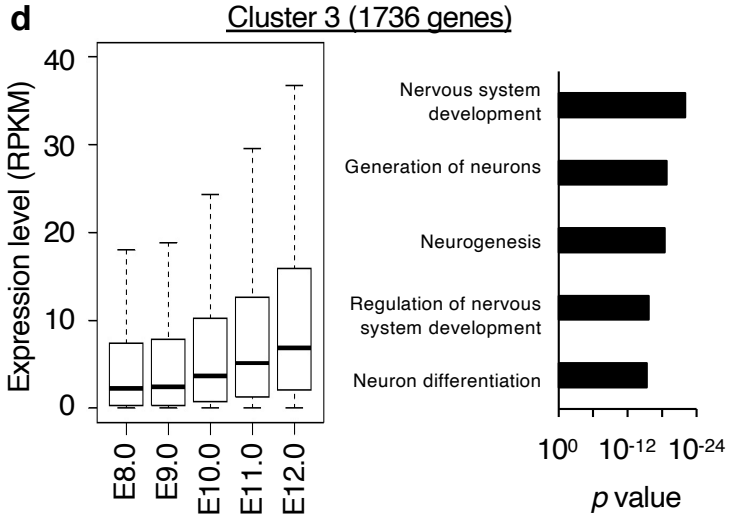

e

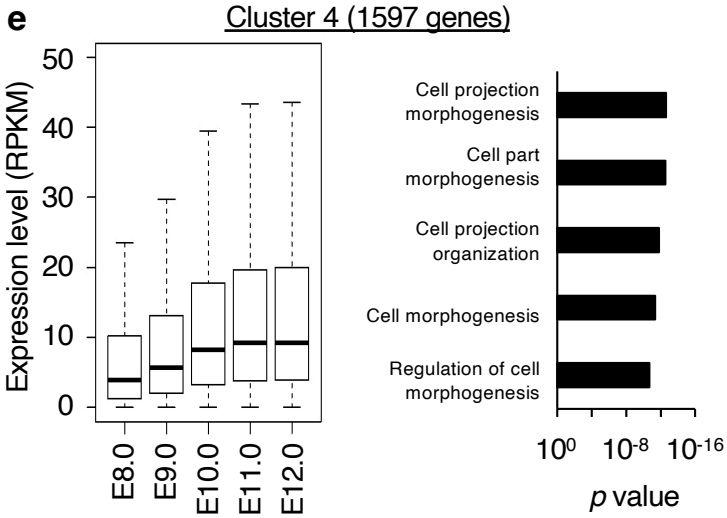

f

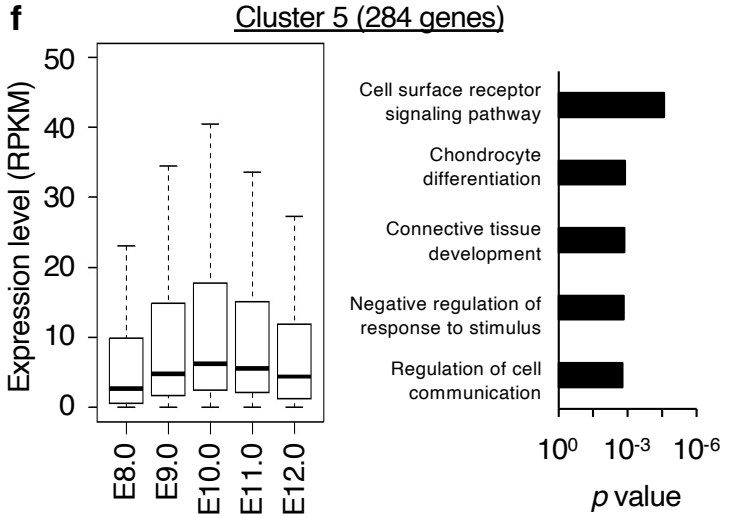

g

Gene symbol	Expression level (RPKM)
Atp5a1	339
Hmga2	279
Lrrn1	217
Calm3	129
Ccnd1	127

h

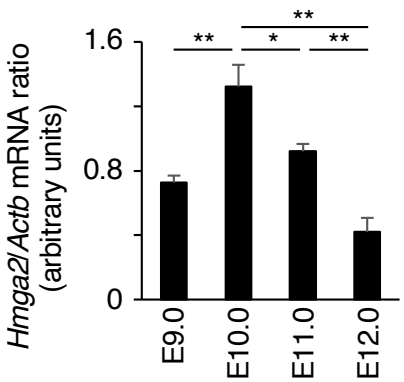

Fig. 4

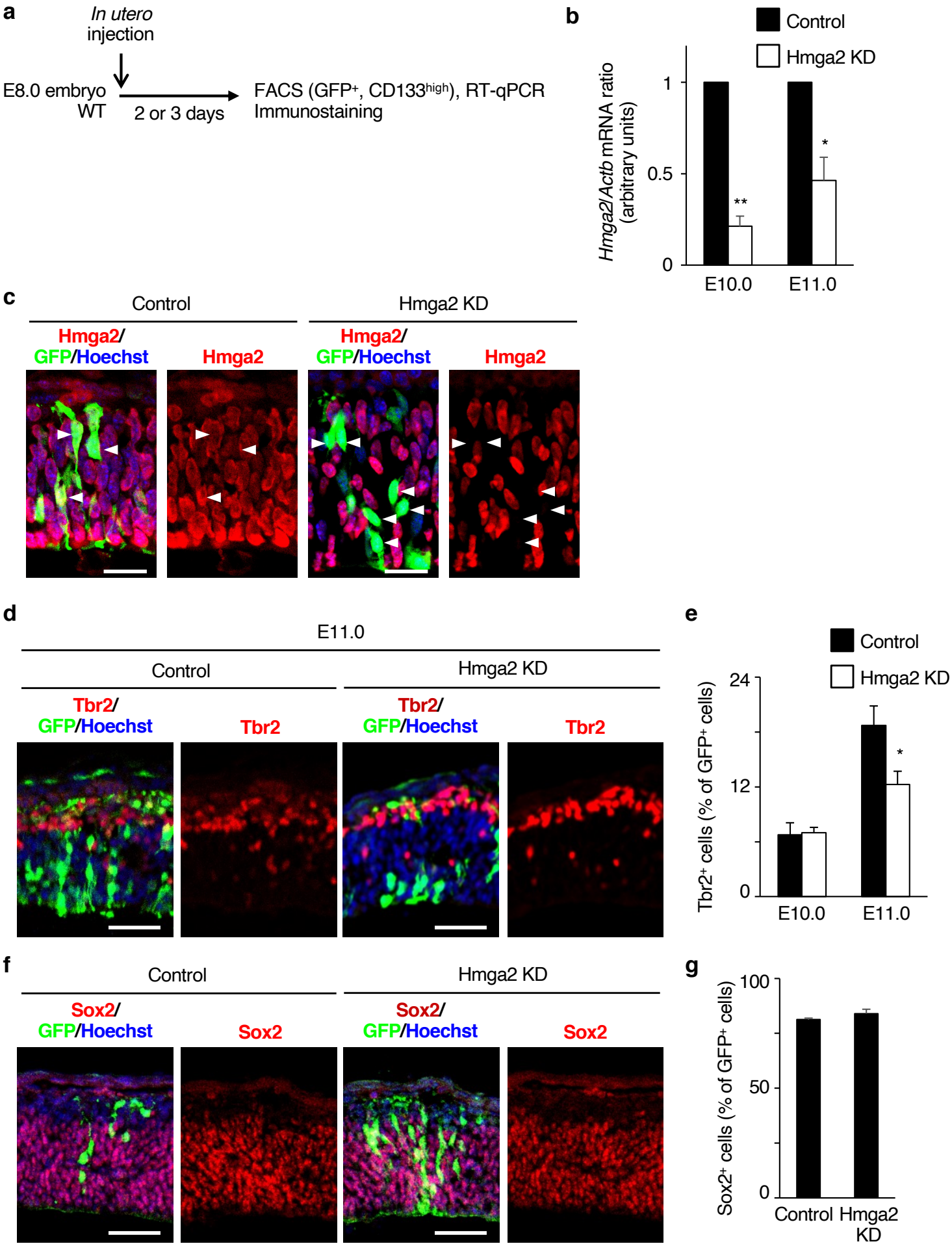
a
In utero injection
E8.0 embryo WT
2 or 3 days
FACS (GFP+, CD133high), RT-qPCR
Immunostaining
b
Control
Hmga2 KD
Hmga2/Actb mRNA ratio (arbitrary units)
1
0.5
0
**
*
E10.0
E11.0
c
Control
Hmga2 KD
Hmga2/ GFP/Hoechst
Hmga2
Hmga2/ GFP/Hoechst
Hmga2
d
E11.0
Control
Hmga2 KD
Tbr2/ GFP/Hoechst
Tbr2
Tbr2/ GFP/Hoechst
Tbr2
e
Control
Hmga2 KD
Tbr2+ cells (% of GFP+ cells)
24
12
0
*
E10.0
E11.0
f
Control
Hmga2 KD
Sox2/ GFP/Hoechst
Sox2
Sox2/ GFP/Hoechst
Sox2
g
Sox2+ cells (% of GFP+ cells)
100
50
0
Control
Hmga2 KD

Fig. 5

a

In utero
injection
E8.0 embryo
WT
2 or 3 days
FACS (GFP+, CD133high),
RNA-seq

b

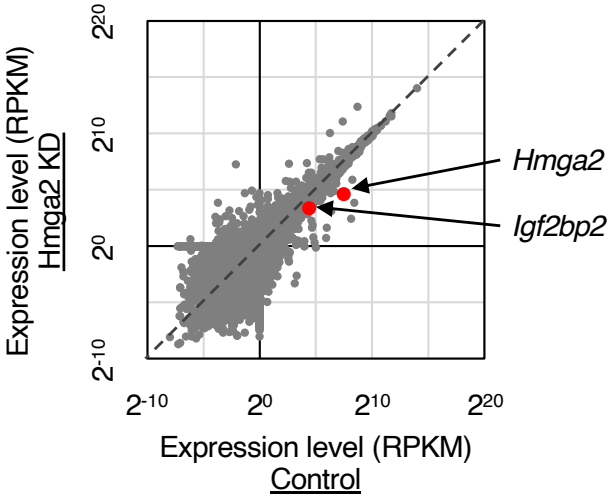
Expression level (RPKM)
Hmga2 KD
Expression level (RPKM)
Control
Hmga2
Igf2bp2

c

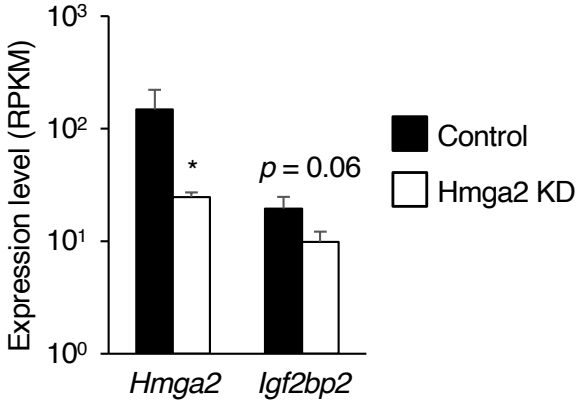
Expression level (RPKM)
*
p = 0.06
Control
Hmga2 KD
Hmga2
Igf2bp2

d

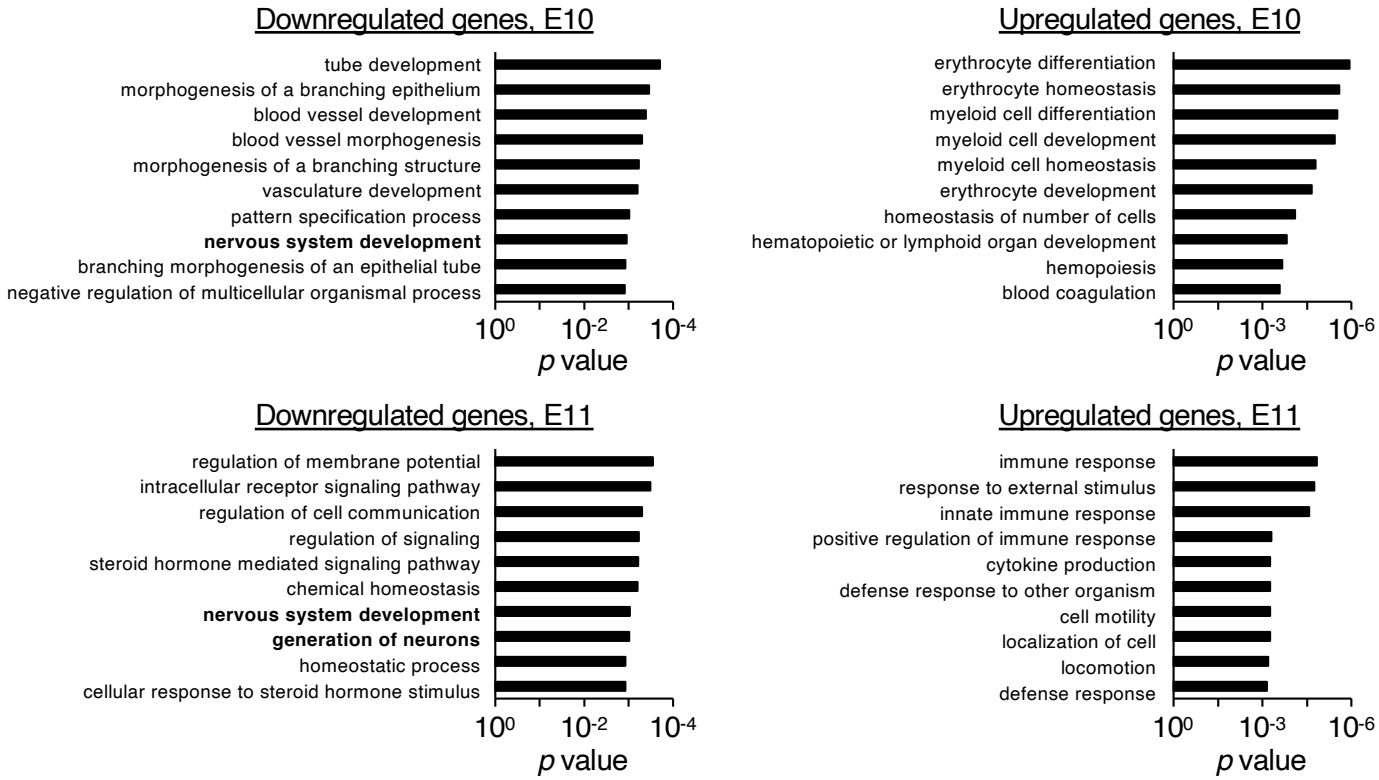
Downregulated genes, E10
tube development
morphogenesis of a branching epithelium
blood vessel development
blood vessel morphogenesis
morphogenesis of a branching structure
vasculature development
pattern specification process
nervous system development
branching morphogenesis of an epithelial tube
negative regulation of multicellular organismal process
p value
Upregulated genes, E10
erythrocyte differentiation
erythrocyte homeostasis
myeloid cell differentiation
myeloid cell development
myeloid cell homeostasis
erythrocyte development
homeostasis of number of cells
hematopoietic or lymphoid organ development
hemopoiesis
blood coagulation
p value
Downregulated genes, E11
regulation of membrane potential
intracellular receptor signaling pathway
regulation of cell communication
regulation of signaling
steroid hormone mediated signaling pathway
chemical homeostasis
nervous system development
generation of neurons
homeostatic process
cellular response to steroid hormone stimulus
p value
Upregulated genes, E11
immune response
response to external stimulus
innate immune response
positive regulation of immune response
cytokine production
defense response to other organism
cell motility
localization of cell
locomotion
defense response
p value

e

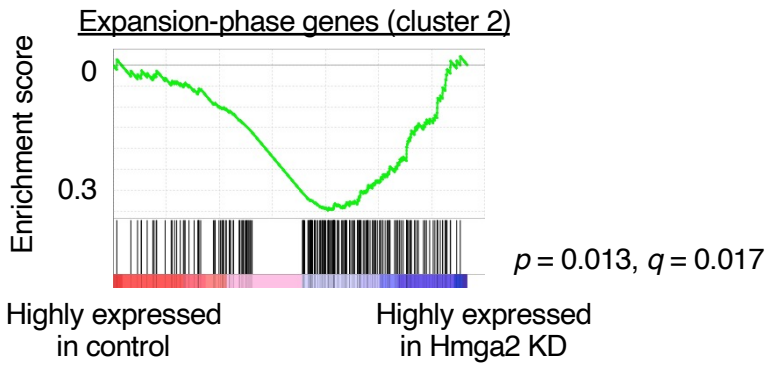
Expansion-phase genes (cluster 2)
Enrichment score
0
0.3
p = 0.013, q = 0.017
Highly expressed
in control
Highly expressed
in Hmga2 KD

Supplementary Fig. 1

a

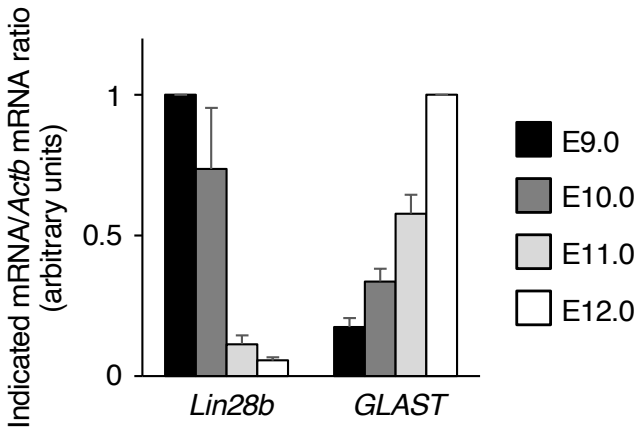

Supplementary Fig. 2

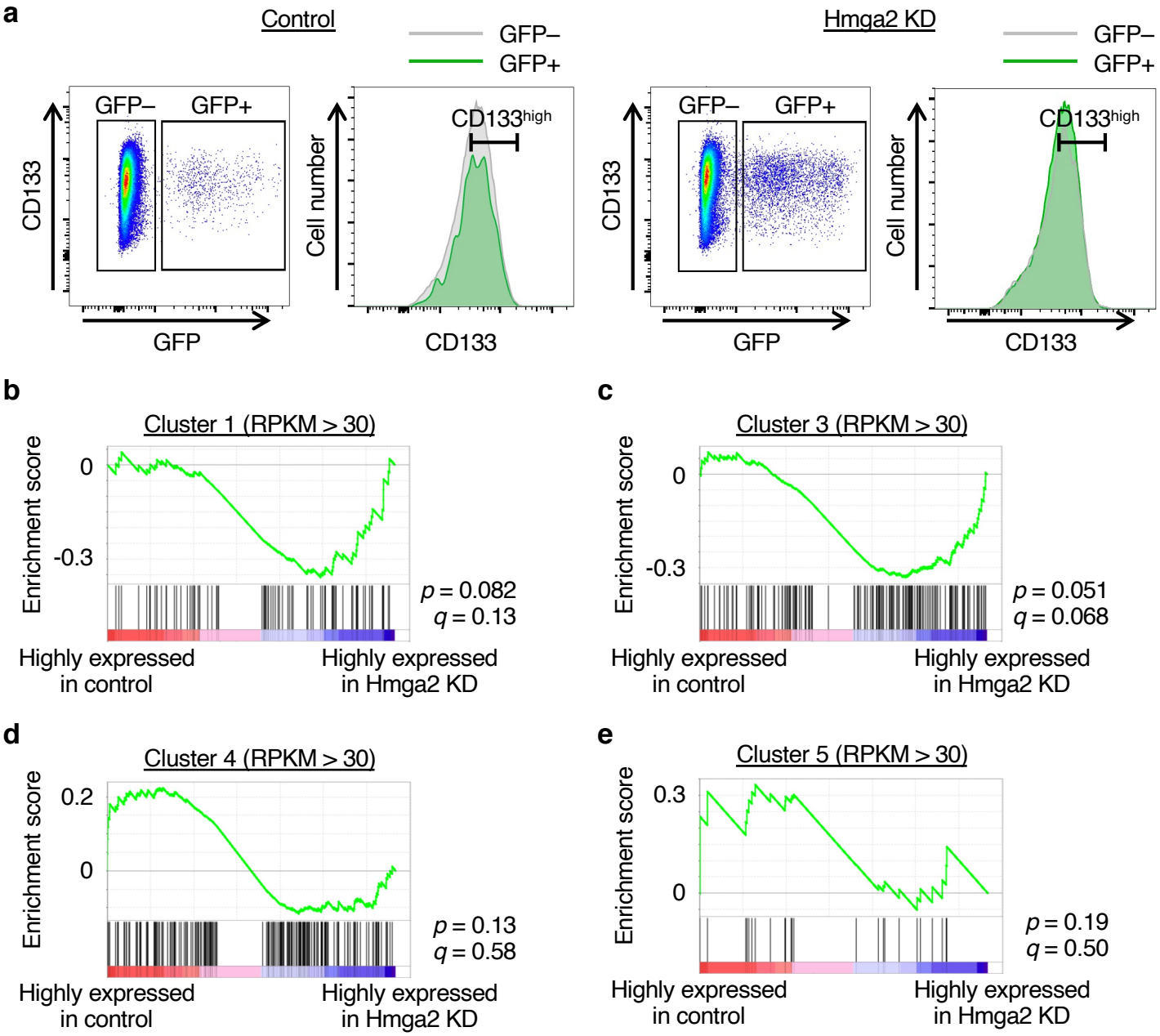

f

Upregulated genes in both E10 and E11

Ensembl gene ID	Gene symbol
ENSMUSG00000053070	*9230110C19Rik*
ENSMUSG00000098112	*Bin2*
ENSMUSG00000026815	*Gfi1b*
ENSMUSG00000095217	***Hist1h2bn***
ENSMUSG00000028678	*Kif2c*
ENSMUSG00000049382	*Krt8*
ENSMUSG00000028581	*Laptm5*
ENSMUSG00000031004	***Mki67***
ENSMUSG00000056234	*Ncoa4*
ENSMUSG00000020120	*Plek*
ENSMUSG00000027074	*Slc43a3*
ENSMUSG00000027500	*Stmn2*
ENSMUSG00000033685	*Ucp2*

Supplementary Fig. 3

a Hmga2 (CPM; 0-3.0)

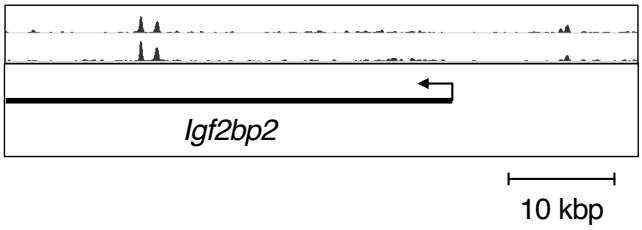

b Hmga2 (CPM; 0-2.0)

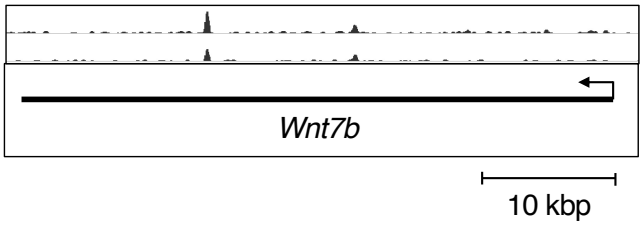

c Hmga2 (CPM; 0-2.0)

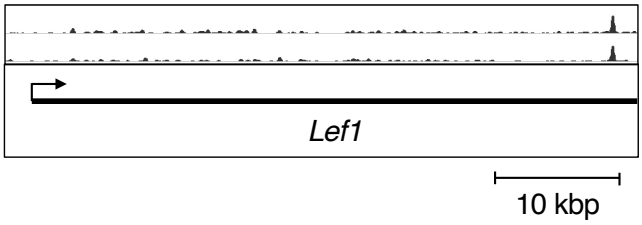
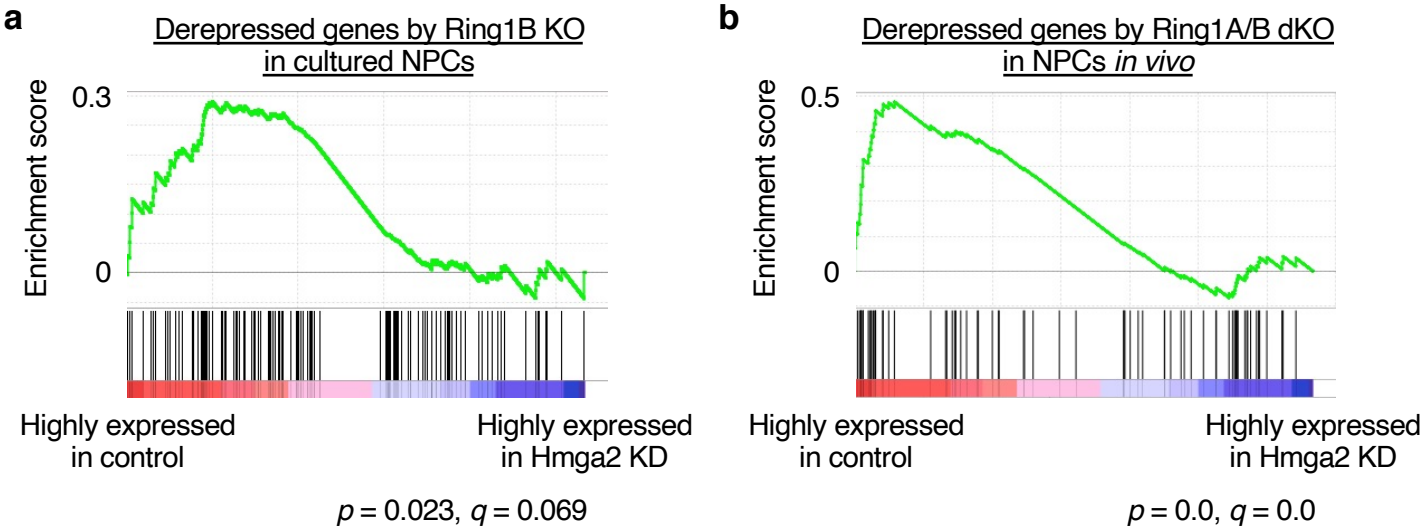
Supplementary Fig. 4